Chapter 10
NIR Light-Sensitive Plasmonic Gold Nanomaterials for Cancer Photothermal and Chemotherapy Applications

Nagamalai Vasimalai

Abbreviations

AIDS	Acquired immune deficiency syndrome
AuNCGs	Gold nanocages
AuNCs	Gold nanocluster
AuNRs	Gold nanorods
AuNS	Gold nanoshell
AuNS	Magnetic gold nanoshell
AuSrs	Gold nanostars
AuTNC	Tetrahedral nanocage
cm	Centimeter
cw	Continuous wave irradiation
DNA	Deoxyribonucleic acid
DOC	Docetaxel
DOX	Doxorubicin
EB	Ethidium bromide
em	Emission
EthD-1	Ethidium homodimer
EW	Egg white
ex	Excitation
EY	Egg yolk
F-AuNRs	Folate-conjugated AuNRs
FBS	Fetal calf serum
FDG	Fluorodeoxyglucose

N. Vasimalai (✉)
INL – International Iberian Nanotechnology Laboratory,
Av. Mestre José Veiga, 4715-330, Braga, Portugal
e-mail: vasimalai.gri@gmail.com; vasi.malai@inl.int

F.L. Deepak (ed.), *Metal Nanoparticles and Clusters*,
https://doi.org/10.1007/978-3-319-68053-8_10

fs	Femtosecond
GEM	Gemcitabine
GSH	Glutathione
HAuNSs	Hollow gold nanospheres
ICG	Indocyanine green
IR	Infrared
MC-AuNS	Microcapsule-coated AuNS
MPB-AuNCs	Methyl-3-propylimidazolium bromide capped AuNCs
MRI	Magnetic resonance imaging
MSA	Mercaptosuccinic acid
$mSiO_2$	Mesoporous silicon dioxide
MSN	Mesoporous silica nanoparticles
MUA	Mercaptoundecanoic acid
mW	Milliwatt
NIR	Near-infrared
nm	Nanometer
NP	Nanoparticle
OCT	Optical coherence tomography
PAH	Poly(allylamine hydrochloride)
PDT	Photodynamic therapy
PEG	Polyethylene glycol
PEI	Polyethyleneimine
PL	Photoluminescence
PLGA-HAuNSs	Poly(lactic-co-glycolic acid)-hollow gold nanoshells
pNIPAAm	Poly-(N-isopropylacrylamide)
ppt-AuNCs	Pentapeptide capped AuNCs
PTT	Photothermal therapy
PVA	Polyvinyl alcohol
ROS	Reactive oxygen species
TEM	Transmission electron microscopy
UV	Ultraviolet
W	Watt
WHO	World health organization
μM	Micromolar

10.1 Introduction

Cancer is the second most dangerous disease in the world after AIDS. In 2015, about 8.8 million deaths worldwide had been reported by the World Health Organization (WHO) [1]. The most common cancer deaths are caused by lung cancer (1.69 million deaths), stomach cancer (754,000 deaths), liver cancer (788,000 deaths), breast cancer (571,000 deaths), and colorectal cancer (774,000 deaths). Worldwide, almost one in six deaths is due to cancer. The number of new cancer cases will rise to 22 million within the next two decades. More than 60% of the world new cancer

cases occur in Africa, Asia, and Central and South America. Seventy percent of the world cancer deaths also occur in these regions.

Cancer can develop anywhere in the human body, when cancer grows in human body, it can perturb the normal cell growth. The tumors are abnormal new growth of cells, and it can grow faster than the normal cells, and the grown tumors can damage the normal cells. There are more than 100 types of known cancers [2]. Among them, *carcinoma is* commonly formed by epithelial cells. *Sarcomas* can form in bones and soft tissues, including lymph, muscle, and blood vessels. *Leukemia* begins in the bone marrow and it does not form solid tumors. *Lymphoma* is a group of blood cancer and *multiple myeloma* is formed in plasma cells. *Melanoma* is the cancer commonly formed in the skin and also pigmented tissues. *Germ cell tumors* are a type of tumor that can be formed in sperm or eggs, and *neuroendocrine tumors* are formed in hormones, and this cancer can produce the higher amount of hormones than the normal amount. *Carcinoid tumors* are a neuroendocrine-type cancer and can spread to the liver and other body organs. Uncontrolled growth of cancer is a death threat to human beings [2]. Therefore, efficient treatment is an essential strategy to curb the growth of cancer cells to save lives.

Chemotherapy and photothermal therapy (PTT) are emerging therapeutic tools to control the cancer cells' growth. Chemotherapy method is commonly used to bio-distribute anticancer drugs to kill the cancer cells. But, uncontrolled release of anticancer drugs can produce cardiac toxicity because of their non-specific drug distribution. However, the nanotechnology provides a solution to selectively kill the cancer cells. Generally, nanomaterials can be used to curb the cancer cells and transport anticancer drugs and also unharmed to the normal cells.

PTT has also been considered as an alternative therapeutic tool to treat solid tumors. Recently, near-infrared (NIR) absorbance gold nanomaterials are extensively used for PTT and bioimaging applications because these NIR absorbance nanomaterials can deeply penetrate to the tissue and reach the cancer cells. These NIR-absorptive nanomaterials can be transduced into local heat and used to treat the cancer cells by PTT. The PTT and chemotherapy combined therapy (chemophotothermal therapy) has been outstanding contribution to the elimination of cancer cells. Since the treatment which combines PTT and chemotherapeutic drugs produces enhanced result and it is highly efficient compared with either individual cancer treatment [3–6].

Generally, there are two biological NIR window regions, such as 700–950 nm (first NIR window) and 1000–1350 nm (second NIR window). Maximum radiative penetration can be achieved by increasing tissue transmission along with decrease in autofluorescence [7]. In particular, the second NIR window (1000 and 1350 nm) can provide a relatively higher efficiency of tissue penetration than the first NIR window. For example, blood is suitably transparent to the rays for second NIR window. The NIR-active nanomaterials after loading the anticancer drugs will specifically reach to target cancer cells. During the NIR laser irradiation, the anticancer drugs can effectively release due to the generation of local heat by NIR-active nanomaterials. Hence, the development of NIR-sensitive gold nanomaterials for biomedical studies has recently attracted a large amount of attention due to the remarkable advances of these materials compared with small organic dyes and inorganic fluorescent nanomaterials.

Gold nanomaterials are of great interest due to their unique physicochemical properties. The NIR light-sensitive gold nanomaterials such as gold nanoshells, gold nanorods, gold nanocages, hollow gold nanospheres, gold nanostars, and gold nanoclusters have been used extensively to kill the cancer cells by PTT and chemotherapy. In this book chapter, I have described the different plasmonic-structured gold nanomaterials and their applications for cancer treatment by using PTT and chemotherapy.

10.2 NIR Light-Sensitive Plasmonic Gold Nanomaterial-Based Cancer Therapy

The gold nanomaterials are poised to make significant contributions to kill the diagnosed cancer cells. It is well known that gold nanomaterials are taking advantages of low toxicity, biocompatibility, and chemical inertness [3]. The plasmonic gold nanomaterials can strongly absorb NIR light and produce heat upon NIR laser irradiation. Further, the localized surface plasmon resonance, which is shape and size dependent, can be triggered by these gold nanomaterials, and it is related to oscillation of free electron in conduction band [8]. Due to the electron-electron and photon-electron interaction during the NIR laser irradiation into plasmonic gold nanomaterials, heat can be generated. The produced heat can be used for PTT and chemotherapy systems [9]. The desirable physical and chemical properties of plasmonic gold nanomaterials make them a prospective candidate for cancer diagnosis and treatments. The morphology and size-tuned NIR-sensitive gold nanomaterials such as Au nanoshells, Au nanorods, Au nanocages, hollow Au nanospheres, Au nanostars, and Au nanocluster are extensively used by researchers for PTT and chemotherapeutic applications (Fig. 10.1) [3, 10–19].

The nanoparticle external incentives have been exploited for such applications, including light, ultrasound, electricity, and magnetic field. Among them NIR light has become attractive due to better penetration to the cells. Further, these NIR light-sensitive gold nanomaterials can be used for controlled release of anticancer drugs in cancer chemotherapy applications. The combined PTT and chemotherapy, which is simultaneous delivery of drugs by heat, is highly needed for cancer therapy. Researchers are attracted by modification of plasmonic gold nanomaterials with targeting ligand for PTT and chemotherapeutic treatment of cancer cells [20].

On the other hand, the development of gold fluorescent nanomaterials for biomedical applications especially bioimaging applications has received much attention. Generally gold nanoclusters can exhibit the fluorescence from UV to NIR regions. NIR or red fluorescent gold nanoclusters have great attention, because of their good biocompatibility and deep penetration to the cells, and it can reduce the autofluorescence of cells [21]. The aim of this book chapter is to provide a summary of recent trend of plasmonic gold nanomaterial-based PTT and chemotherapy, and the discussion was divided into the following subheadings such as Au nanoshells, Au nanorods, Au nanocages, hollow Au nanospheres, Au nanostars, and Au nanoclusters.

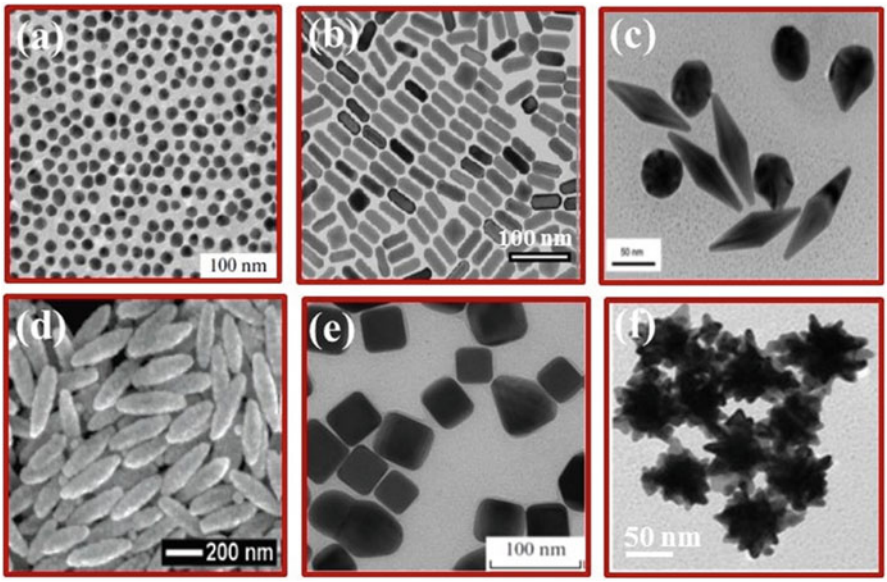

Fig. 10.1 Various types of plasmon-resonant nanoparticles: (**a**) 16 nm nanospheres [10], (**b**) gold nanorods [11], (**c**) gold bipyramids [12], (**d**) gold nanorice, [13], (**e**) gold nanocubes [14], and (**f**) gold nanostar [15] (Reprinted by permission from Springer [Colloid J] 73, 118–127, Copyright 2011; American Chemical Society [Chem. Mater] 25, 555–563, Copyright 2013; American Chemical Society [J. Phys. Chem. B] 109, 22192–22200, Copyright 2005; American Chemical Society [Nano Lett.] 6, 827–832, Copyright 2006; Springer [Nanotechnologies in Russia] 5(7–8), 454–468, Copyright 2010; Elsevier [Colloid Interface Sci.] 16, 118–127, Copyright 2011)

10.2.1 Au Nanoshells for PTT and Chemotherapy Applications

Au nanoshells (AuNSs) can be prepared by three ways, such as (1) growing on silica nanoparticle, (2) polymer nanoparticles, and (3) prepared from Ag nanoparticles by galvanic replacement. The AuNS can convert an absorbed light into heat with efficacy. The cross-sectional absorption of nanoshells is six orders of magnitude larger than indocyanine green dye, making this material a much stronger NIR absorber. Therefore, AuNS acts as more effective photothermal coupling agent [13]. In addition, the AuNS absorption properties are dependent upon the nanomaterials' rigid metallic nature rather than the more labile molecular orbital electronic transitions of organic dyes. This makes AuNS less susceptible to photobleaching, a problem commonly associated with conventional dyes [22]. Hence, the AuNS are extensively used for PTT and imaging applications due to their NIR absorbance and the scattering properties. Since the seventeenth century, the thermal treatment of tumor cells has become one of the major methods in tumor therapy [23]. Hirsch et al. for the first time used AuNS for PTT in 2003. SH-PEG-coated gold-silica nanoshell was prepared by wet chemical method and exhibited a broad absorption

peak from 550 to 1050 nm. For PTT application, the human breast epithelial carcinoma SK-BR-3 cells were treated with gold-silica nanoshell of 20 nm size, and it was irradiated with 820 nm laser with a power density of 4 W/cm^2. Tumor cells were selectively destroyed by the treatment of gold-silica nanoshell with NIR laser irradiation [24].

Loo et al. have reported the synthesis of antiHER2 and PEG coated SiO_2@AuNS, denoted as antiHER2-AuNS for cancer inhibition studies. For in vitro study, antiHER2-AuNS with SKBr3 human breast adenocarcinoma cells exposed with 820 nm for 7 min with a power density of 0.008 W/cm^2. AntiHER2-AuNS incubated with SKBr3 cells and exhibited higher scattering than the nontargeted AuNS. PTT study was carried out in AuNS with targeting peptide of A54. The A54 peptide displayed the targeting ability for liver cancer cells. The modification A54 with AuNS was linked through amino acids and cysteine-containing thiol group. This thiol group functionality can covalently bind with AuNS shell. The targeting capability of A54-AuNS was performed with HL-7702 normal liver cells and BEL-7404 and BEL-7402 human heptacellular cancer cells. After NIR laser irradiation for 7 min, the green fluorescence was clearly observed in normal HL-7702 cells, whereas no fluorescence was observed in cancer cell lines of BEL-7404 and BEL-7402, because the live cells only can emit the fluorescence. These results revealed that the cancer cells had more uptake of AuNS, and it kills more cancer cells than the normal cells, due to the high affinity of A54 peptide. NIR laser irradiation induced the cancer killing ratio without destruction of the normal cells. In TEM, the microvilli-like structure was observed for the case of BEL-7404 cells treated with the A54-AuNS in the nuclei and cell membranes. The cancer cell apoptosis was observed by flow cytometry, after the few min of NIR light irradiation [25].

In addition, West and co-workers have developed PEG/AuNS-based vivo imaging and therapy. The PEG-AuNSs were intravenously injected to CT26 murine colon tumors in mice. After 20 h circulation of the PEG-AuNS with cancer and normal cells, the cells were imaged by optical coherence tomography (OCT). Finally, the signal of PEG-AuNS in cancer cells was found by OCT, whereas no signals were found in normal cells. Then, the cancer cells were irradiated with NIR laser with a power density of 4 W/cm^2, and it was found that the size of cancer cells decreased [26]. In another research group, dendrimer porphyrin-coated AuNS was used for PTT. AuNS was coated on the silica shell, which is the layer-by-layer coating of dendrimer porphyrin, and then the AuNS was enlarged by hydroxylamine seeding. The PTT efficiency was measured by 808 nm NIR laser irradiation. After 5 min irradiation, temperature was reached to 50 °C, and this is due to the gold shell layer. The dendrimer porphyrin-coated gold nanoshells was incubated with HeLa cells and irradiated to 5 min with NIR laser. This approach was proved to kill the more cancer cells (Scheme 10.1 and Fig. 10.2) [27].

Further, Gao and co-workers have synthesized pH-sensitive liposomes and chitosan-coated AuNS (AuOL) for PTT. The particle size was calculated to be 172 nm by TEM, and the zeta potential was 20.7 mV. Oleanolic acid which exhibits antitumor property was used for controlled release to cancer cells. Controlled release of anticancer drugs was observed at pH 7.4, whereas rapid release was found at

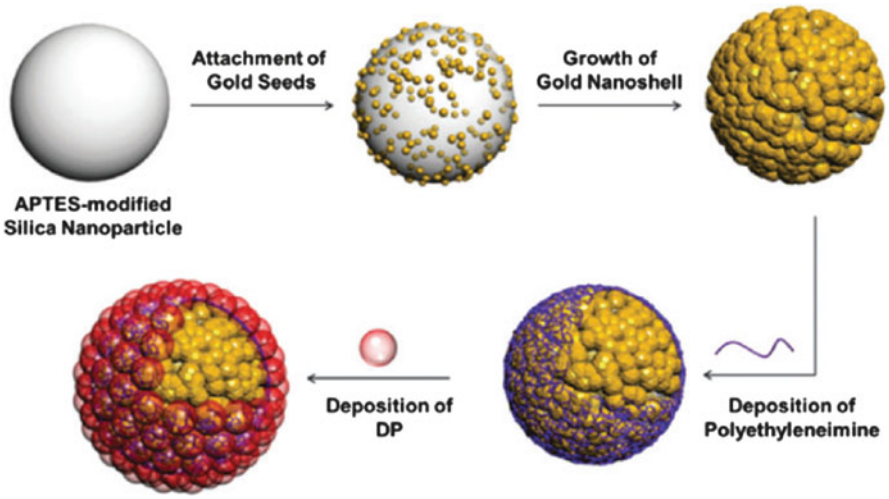

Scheme 10.1 Schematic illustration of the preparation of the multilayered nanoparticles consisting of AuNS and dendrimer porphyrin on the silica nanoparticles (Reprinted by permission from The Royal Society of Chemistry [Chemical Communications] 52, 1258–1261, Copyright 2016)

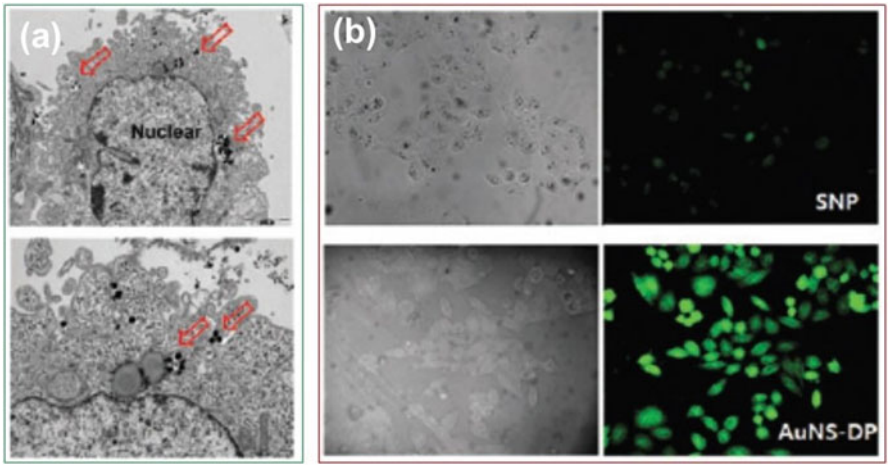

Fig. 10.2 In vitro observations of AuNS-DP-treated cells. (**a**) TEM images of HeLa cells treated with AuNS-DP and (**b**) fluorescence and optical images indicating ROS generation in HeLa cells treated with AuNS-DP and light irradiation (Reprinted by permission from The Royal Society of Chemistry [Chemical Communications] 52, 1258–1261, Copyright 2016)

pH 5.4. To evaluate the antitumor effect with NIR laser irradiation, the AuOL treated with 143B cancer cells have shown to kill more cancer cells in the presence of oleanolic acid. The AuOL-coated oleanolic acid-mediated tumor therapy is a potential candidate for PTT and chemotherapy applications [28]. Moreover, Tang

et al. reported the synthesis of multifunctional AuNS on silica nanorattles; firstly, 120 nm of silica nanorattles (SNs) were treated with 1–3 nm size gold seeds as described in the literature [29]. Gold first attached to amine group of SNs, and the resultant GSN was further treated with K_2CO_3 and gold chloride solution and then subsequently treated with hydroxylamine hydrochloride solution. It was noted that the color of the solution changed from colorless to bluish green, and it indicated the formation of nanoshells. Further, PEG also was coated for biocompatibility (pGSN). The obtained pGSN was applied for combined chemophototherapy. For PTT, the pGSNs were treated with hepatoma 22 (H22) under NIR laser irradiation with a power density of 2 W/cm^2. They have monitored the anticancer drug of docetaxel (DOC), the cumulative DOC release was found in 1/20 h, and it was revealed that the 60% of drug was released within 1 week. For in vitro cytotoxicity test, 3-(4,5-dime-thylthiazol-2-yl)-2,5-diphenyltetrazolium bromide (MTT) assay was used. The DOC-loaded pGSNs (DOC-pGSNs) were irradiated with NIR laser and revealed that the NIR-irradiated DOC-pGSNs effectively killed cancer cells compared to the DOC-pGSNs without NIR irradiation. In vivo study also confirmed that the combined PTT and chemotherapy were killed approximately 70% of cancer cells [30].

The same research group also modified pGSNs with target of transferrin (Tf-pGSNs) and tested the targeting and PTT efficacy. The Tf-pGSNs was treated with MCF-7 cancer cells, and 808 nm NIR laser was irradiated with power density of 2 Wcm^{-2}. The obtained results confirmed the selective targeting ability and PTT efficacy of Tf-pGSNs. These two nanomaterials are around 130 nm in size, and it can be easily excreted by urine from the body [31]. Further, Chu and co-workers also prepared the liposome-functionalized pGSNs (Li-pGSNs) with a particle size of 238 nm. The doxorubicin (DOX)-loaded Li-pGSNs (DOX-Li-pGSNs) killed more human liver cancer cells (SMMC-7721) with the 808 nm NIR laser irradiation, and it suggested that the Li-pGSNs have directly delivered DOX and are sensitive to PTT [32]. Further, Yoo and co-workers have prepared a half-AuNS (H1-AuNSs), and coated with poly(ethylene glycol)-poly(lactic-co-glycolic acid) and anticancer drug of DOX was loaded, which is denoted as (DOX-PEG-PLGA@AuNSs). These DOX-PEG-PLGA@AuNSs were applied for chemophotothermal therapy applications. The H1-AuNs exhibit the broad absorption band at 790 nm. The DOX-PEG-PLGA@AuNSs were intravenously injected into A431 tumor-bearing mice. DOX was released during the irradiation of 808 nm laser with a power density of 2.56 W/cm^2. The obtained bioimages also confirmed that the AuNSs are accumulated in tumor. The cancer cells were died due to the simultaneous effect of PTT and DOX release, and this was confirmed by in-vivo studies [33].

Due to unique physical and chemical properties of silica NPs (SiO_2) that have made an attractive material and are being applied for biomedical, drug delivery applications. Choi et al. reported the SiO_2@Au phagocytosed through the monocytes (monocyte AuNS), and it was ablated during the fs laser irradiation ($\lambda = 754$ nm; 1.54 W of power density). The reaching ability of monocyte AuNS to the hypoxia tumor was lower during the chemotherapy, but in vitro model tumor spheroid creates a selective environment for hypoxia tumor. The spheroid layer was found in the surrounding of hypoxia cells. The monocytes and AuNSs were incubated with spheroids in cell culture plate and disseminated the tumor spheroids to reach interior hypoxia cells. Monocyte AuNS produced the effect of PTT ablation, while fs laser irradiation, causing the death of cancer cells [34].

In addition, Kim et al. also reported the silica core and iron oxide nanoparticle-coated AuNSs for PTT and MRI applications. First, 100 nm of silica spheres were prepared and modified their surface with 3-aminopropyltrimethoxy, and then 2-bromo-2-methylpropionic acid-coated Fe_3O_4 nanoparticles [35], where the covalent bond was formed through the nucleophilic reaction between bromo and amino groups. Then, 1–3 nm size of gold seed was attached through to amine group of modified silica sphere. Finally, SiO_2@Fe_3O_4@AuNS (Fe_3O_4@AuNS) are produced. The Mag-AuNS exhibited the broad absorption in NIR range. The targeting antibody, antiHER2/neu, was treated to Mag-AuNS (anti-Mag-AuNS). The anti-Mag-AuNS positive was tested with SKBR3 human breast cancer cells, and antiHER2/neu-negative was treated with A520 lung cancer cells. In the in vitro MR images, antiHER2-Mag-AuNS treated with SKBR3 is darker than antiHER2-AuNS treated with A520 cells. The in vitro PTT studies showed that after the irradiation of NIR pulse laser with power density of 20 mW, SKBR3 cells. Treated with antiHER2-AuNS were died, whereas A530 cells treated with antiHER2-AuNS were died after the irradiation of 60 mW laser power 60 mW laser power [36].

Similar approach also was followed by Ji et al.; the Fe_3O_4@SiO_2@Au was synthesized by wet chemical method, and it was conjugated with thiolated PEG and adsorbed on the surface of gold. The resultant PEG-Fe_3O_4@SiO_2@Au have shown the broad absorption peak from 825 to 910 nm. In MRI, a dark T_2-weighted phantom was observed with the increased concentration of PEG-Fe_3O_4@SiO_2@Au. To investigate the temperature elevation induced by NIR laser on PEG-Fe_3O_4@SiO_2@Au, a continuous-wave fiber-coupled diode laser with an 808 nm wavelength was used. At a concentration of 7.5×10^{12} particles/mL, an elevation of 16.3 °C was achieved with a power output of 1 W [37]. Moreover, gold nanoparticles assembled silicon nanowires (AuNPs@SiNWs) was developed for PTT applications by Su et al. The AuNPs@SiNWs showed the broad absorption from 700 to 1000 nm. After irradiation of 808 nm laser on AuNPs@SiNWs for PTT, the temperature was reached to 60 °C within 3 min of laser irradiation with low power density (2 W/cm^2). Further, SiNW@AuNPs was coated with PEG (denoted as SiNW@AuNPs-PEG) for in vitro applications. The human lung carcinoma cells (A549 cells) and human epithelial cervical cancer cells (HeLa cells) were treated with SiNW@AuNPs-PEGs and irradiated with 808 nm laser for 3 min; as a result, cancer cells were completely destroyed (Fig. 10.3) [38].

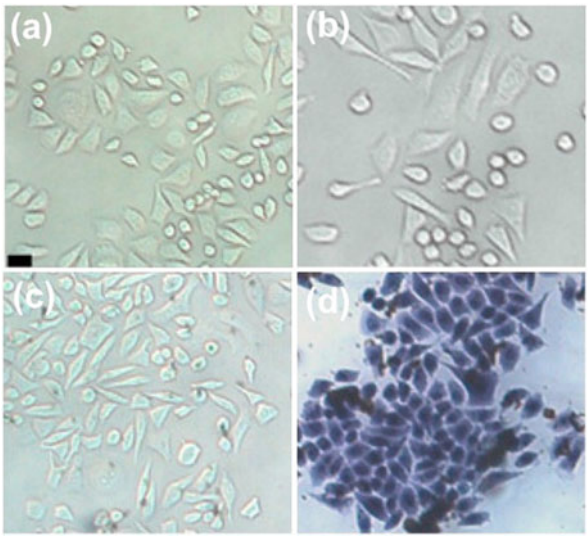

Fig. 10.3 Optical images of KB cells. (**a**) Control cells, (**b**) control cells after laser irradiation, (**c**) cells cultured with 150 μg/mL PEG-AuNPs@SiNWs, and (**d**) cells cultured with 150 μg/mL PEG-AuNPs@SiNWs after 3 min 2 W/cm^2 808 nm laser irradiation. *Blue color* indicates dead cells (trypan blue test). Scale bar = 20 μm (Reprinted by permission from American Chemical Society [Nano Letters] 12, 1845–1850, Copyright 2012)

Bardhan et al. have developed a multifunctional AuNS (Au@SiO_2) demonstrating a PTT, MRI, and IR imaging. The Au@SiO_2 showed the absorption band at 820 nm. The Au@SiO_2 further modified with iron oxide and the fluorophore of (indocyanine green) ICG, as a result of a high T2 relaxivity (390 mM^{-1} s^{-1}) and the ICG fluorescence enhancement. For in vitro study, AuNS@Fe_3O_4@SiO_2-ICG was conjugated with antiHER2, and it can be targeted to the HER2-positive SKBR3 cancer cells. After the treatment of antiHER2-AuNS@Fe_3O_4@SiO_2-ICG with HER2-positive SKBR3 and HER2-negative MDA-MD-231 human breast cancer cells, the SKBR3 cells produced intense MR signals than the MDA-MD-231 cells. The antiHER2-AuNS@Fe_3O_4@SiO_2-ICG-treated SKBR3 cells showed an IR fluorescence for in vitro IR images, whereas antiHER2-negative MDA-MD-231 cells have not shown IR fluorescence. For in vitro PTT, the SKBR3 cells treated with antiHER2-AuNS@Fe_3O_4@SiO_2-ICG were totally demolished under irradiation of 808 nm laser with 3.72 W/cm^2 [39]. These results demonstrated that the MRI and PTT produced the more efficacy to kill the cancer cells.

Compared with traditional hypothermia method, chemophotothermal therapy has received huge attention. This method not only selectively delivers the drugs but also produces synergistic effect for optimal treatment efficacy and reduces the side effects [28, 30, 32, 33]. Further, the AuNS surface modifications also play a role to increase the efficacy of treatment. Researchers are needed to concentrate the synthesis of second biological window absorption AuNS and to develop chemophotothermal therapy-based multidrug delivery. Further, magnetic nanoparticle-attached mesoporous silica-modified AuNS is also a good choice for the chemophotothermal therapy and MRI applications.

10.2.2 Gold Nanorods for PTT and Chemotherapy Applications

The gold nanorods (AuNRs) are promising materials with superior performances, such as easy functionalization and synthesis, good biocompatibility, and high photothermal efficacy. It is well known that AuNRs have two kinds of peaks such as transverse and longitudinal mode. The longitudinal mode peak appears at NIR region, and it depends on the aspect ratio of AuNRs [40, 41]. They have been proven to be promising in a wide range of biomedical applications such as biomedical imaging, photothermal therapy, photodynamic therapy, and drug or gene delivery. Because the longitudinally localized surface plasmon resonance absorption of AuNRs can be easily adjusted to the range of near-infrared (NIR) light which can penetrate deeply into human tissues with minimal invasion, AuNRs as great nanocarriers and imaging agents reveal a great application prospect for photoacoustic tomography, photothermal therapy, or NIR light-mediated theranostic platform. Further, Huang and co-workers had proposed 11-mercaptoundecanoic acid-PEG-coated AuNRs (MUA-PEG-AuNRs) for the delivery of hydrophobic drug of paclitaxel (PTX). The hydrophobic PTX was entrapped on the surface of MUA-PEG-AuNRs, and it allows the PTX delivery through the lipophilic plasma cell membrane. The PTX@MUA-PEG-AuNRs were incubated with KB-3-1 and A549 cancer cells, and the results revealed that the combined PTT and chemotherapy has shown a higher efficacy to kill the cancer cells [42].

Further, folate-conjugated AuNRs (F-AuNRs) were targeted to malignant KB oral carcinoma cells, and maximum delivery was obtained by the NIR irradiation. The F-AuNRs were applied to culture with KB cells and NIH-3T3 cells, and after 6 h, it was found that there are more F-AuNRs in KB cells than the NIH-3T3 cells. The obtained F-AuNRs adsorption confirming that the folate receptor expression. The femtosecond (fs) pulse NIR Ti:sapphire laser was used for PTT with a 4.5 mW of laser power. The green fluorescent protein actin expression (GFPactin) was used to image the cells. The blebbing was observed in KB cell membranes, but not near to F-AuNRs. But, in the absence of NIR laser treatment, there was no blebbing on the KB cell membranes. The actin degradation may be hypothesized by the presence of calcium ion in the intracellular region. It was stained with ethidium bromide (EB) after the experiment was carried out and found that calcium-rich-mediated cells shown blebbing but not found in calcium-deficient-mediated cells. The F-AuNR-based PTT produced cavitation because of the influx of the calcium ion, and it produced the blebbing [43].

Moreover, Huang et al. reported that the synthesis of AuNRs with anti-epidermal growth factor receptor (anti-EGFR) monoclonal antibodies and incubated in cell cultures with a nonmalignant epithelial cell line (HaCat) and two malignant oral epithelial cell lines (HOC 313 clone 8 and HSC 3). The anti-EGFR antibody-conjugated AuNRs bind specifically to the surface of the malignant-type cells with a much higher affinity due to the overexpressed EGFR on the cytoplasmic membrane of the malignant cells. Finally, it has been reported that the anti-EGFR-

AuNRs displayed high uptake of the malignant cell line than the nonmalignant cells. Further, increase in an extinction intensity of malignant cells than the nonmalignant cells was observed. In the presence of anti-EGFR-AuNRs with malignant cells, 800 nm continuous wave irradiation (cw) Ti was used to induce the cancer cells, whereas nonmalignant HaCat cells required NIR laser with high power density 20 W/cm^2 to kill the cancer cells [6]. Followed by Tae and co-workers, they have developed the PTT technique with polymer-based AuNRs. In this study AuNRs were modified with chitosan-conjugated pluronic F-68 (Chi-PF68). AuNRs@Chi-PF68 and 780 nm laser were used to irradiate SCC7 squamous carcinoma cells with 41.5 and 26.4 W/cm^2 power densities. Their report revealed that high amount of SCC7 squamous carcinoma cells were killed by AuNRs@Chi-PF68 [44].

Bremer et al. developed AuNR conjugated with metalloprotease and Cy5 dye (P-Cy5) for PTT. Cy5 fluorescence was quenched after conjugated with matrix metalloprotease and AuNRs. After reaching the tumor target, the fluorescence was enhanced due to the release of Cy5 from the AuNR@matrix metalloprotease, and they have performed in vivo imaging study with SCC7 tumor cells. HeLa cells were used for PTT study, and it was noted that temperature was reached to 45 °C within 4 min after irradiate NIR laser [45]. Further, Hauck et al. proposed AuNR-based PTT with three types of cancer cells, such as OCI AML3 human myeloid leukemia cells. First, OCI AML3 human acute myeloid leukemia cells were treated with AuNRs, and then the anticancer drug of cisplatin was loaded, and then PTT efficacy was monitored by the irradiation of NIR laser. The observed proliferation of chemophotothermal therapy-treated cells resulted in a surviving fraction which was 78% lower than chemotherapy treatment alone and 84% lower than hyperthermia alone. These results confirmed that the AuNRs induced the efficacy of PTT and chemotherapy to kill the cancer cells [46]. Interestingly, Zhou et al. reported the zwitterionic phosphorylcholine-coated AuNRs (AuNR@PC) have exhibited the good biocompatibility and solubility, because of their phosphorylcholine zwitterionic property. It was noted that uptake of CNE-1 nasopharyngeal cancer cells by AuNR@PC is three times higher than that of PEG-coated AuNRs. The CNE-1 cancer cells and rhinal epithelial normal cells are treated with AuNR@PCs. The bioimaging study reported that AuNR@PC was located in cytoplasm, whereas there are no AuNRs found in normal cells. These results indicated that the AuNR@PC is selective for cancer cells. For PTT 300 mW power density was used, and their cancer cell images showed the green fluorescence due to illumination of dead cells, whereas normal cells did not illuminate; it confirmed that the PTT effect of AuNR@PCs is selective for CNE-1 cancer cells [40].

Interestingly, Tsai et al. prepared a rod-in-shell AuNR with 50 nm size by seedless method, and it exhibits a second biological NIR window absorbance. The obtained AuNRs were coated with a Ag shell, then, subsequently, the Au/Ag alloy was prepared by galvanic reaction, and then AuNR-in-Au/Ag shell (rattle-like) nanomaterials were prepared. Inner and outer NIR plasmon was produced by a dielectric hollow space. The absorption peaks are observed at 1100 and 1280 nm. For PTT, rod-in-shells were irradiated with a 1064 nm laser (power density of 3 W/cm^2). To reflect this phototransduction efficiency in PTT, the zone area of cell

death was extended beyond the laser illumination region in LLC/LL2 lung cancer cells treated with 2 nm gap structures by administering irradiation using a 1064 nm laser with a 3 W/cm^2 power density. Comparatively, the PTT zone area of cell destruction was not apparent when rod-in-shell with 6.5 nm gap was used to treat LLC/LL2 tumor cells. LLC/LL2 lung cancer cell-bearing mice were intratumorally injected with the rod-in-shells and irradiated by 1064 nm laser with a power density of 3 W/cm^2. The 2 nm-gap rod-in-shells have shown the complete control over the tumor growth, whereas 6.5 nm-gap rod-in-shells have shown no control over tumor growth [47]. Similarly, PEG-coated AuNR (PEG-AuNR) was developed by Maltzahn et al. and applied for PTT. MDA-MB-435 melanoma-type cancer cells were treated with PEG-AuNR and killed the cancer cells by computational mediated PTT [48].

Very recently, Kang et al. have developed the TGN nanocomplex, which was prepared by AuNRs, porphyrin, and trastuzumab. This TGN nanocomplex increased the targeting specificity of HER2-positive breast cancers. NIR laser-irradiated TGN nanocomplex had a selective destruction of HER2-positive breast cancers and inhibited the tumor growth, and this was studied by in vitro and in vivo models. It was discovered that BT474 and SK-BR-3 of human breast cancer cells are strongly bound with TGN nanocomplex. But, the lower cellular uptake was observed in SK-BR-3 than BT474 cancer cells. This might be due to biological environmental differences and the photothermal sensitivity of cancer cells. The TGN provides better cancer killing efficiency than the conventional molecules. This is the first report for the PTT of cancer cells using TGN nanocomplex [49]. Further, Yuan and co-workers have developed novel nanomaterial of gold nanocluster (AuNCs)-coated AuNRs (AuNRs-AuNCs) for PTT. The AuNRs exhibit the longitudinal absorption at 719 nm and transverse at 508 nm. After the incorporation of AuNRs with red emittive AuNCs, the longitudinal absorption at 719 nm was shifted to 786 nm. The photothermal performance of AuNRs-AuNCs was investigated using 808 nm laser with a continuous wave of 2.29 W. The NIR laser irradiation increased the temperature from 28 to 42.9 °C within 300 s irradiation. The AuNRs-AuNCs, photothermal efficacy, and biocompatibility provided great biomedical applications for cancer PTT [50].

Generally, AuNRs have limited specific surface area and are not appropriate for drug delivery applications. Nevertheless, silica-coated AuNRs are a promising material for drug delivery. Zhang et al. have synthesized Au@SiO_2 using CTAB and amino silane with gold chloride solution. In the Au@SiO_2, silica thickness was found to be ~30 nm by TEM, and it exhibited the absorption peak at 760 nm. The DOX was loaded into Au@SiO_2, and then drug was released during the irradiation of 780 nm NIR laser. In vitro drug release studies are carried out at 37 °C. In the absence of laser irradiation, a small amount of drug release was found, whereas the release amount was induced by 780 nm laser irradiation. This is due to the dissociation of electrostatic interaction of DOX and silanol. For in vitro study of A549 human lung carcinoma cells were taken, those cells were treated with DOX-loaded Au@SiO_2. Death ratio of cancer cells was increased by NIR laser irradiation [51]. Later, Yang et al. have synthesized AuNRs@SiO_2 and modified the surface

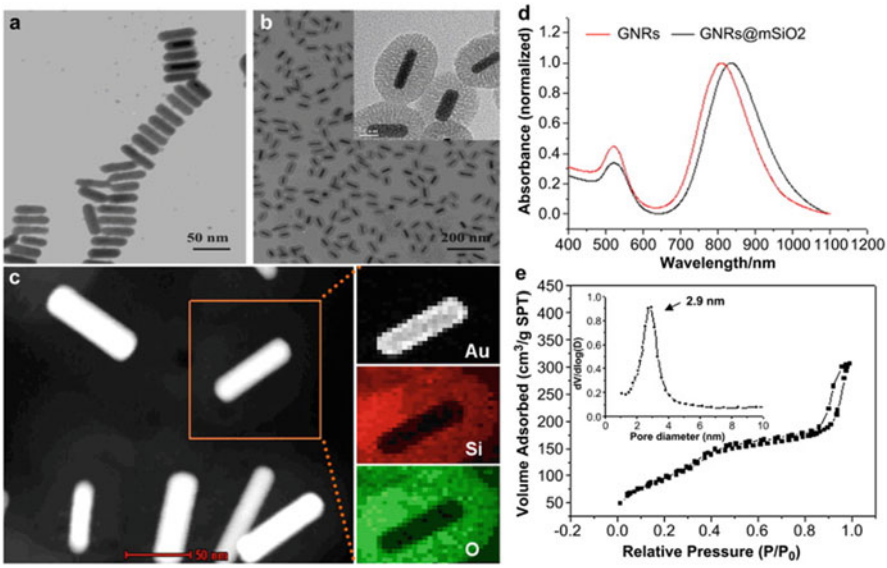

Fig. 10.4 Representative TEM image of (**a**) GNRs; (**b**) the synthesized GNRs@$mSiO_2$ nanomaterials; (**c**) STEM-EDX maps of Au, Si, and O; (**d**) extinction spectra of GNRs and GNRs@$mSiO_2$; and (**e**) N_2 adsorption-desorption isotherms (*inset*: the pore diameter distribution) for GNRs@$mSiO_2$ (Reprinted by permission from American Association for Cancer Research [Biomaterials] 34, 3150–3158, Copyright 2013)

with aptamer DNA. This is the first report for anticancer aptamer AS1411-DNA which is used for capping as well as targeting agent. The AS1411-DNA aptamer is a targeting agent for renal carcinoma cells. Nucleolin is a protein and it is overexpressed in cancer cells [52]. Interestingly, nucleolin can bind with aptamer AS1411-DNA and form a stable G-quadruplex DNA structure. This approach was applied for the drug delivery, and it allows cargo for controlled release of anticancer drugs and induced the apoptosis due to the PTT efficacy [53].

Later, Yang et al. have developed GNRs@$mSiO_2$, and it was conjugated with RGD peptides on the terminal groups of poly(ethylene glycol) (pGNRs@$mSiO_2$-RGD). Then the pGNRs@$mSiO_2$-RGD was used for PTT to deliver the DOX into tumor cells. For in vivo study, A549 cancer cells were incubated with DOX-loaded pGNRs@$mSiO_2$-RGD (DOX- pGNRs@$mSiO_2$-RGD). After the NIR laser irradiation, DOX was released due to the photothermal ablation. Compared with chemotherapy or PTT alone, the combined treatment has shown a higher therapeutic efficacy (Figs. 10.4 and 10.5) [54].

In addition to the mesoporous silica layer incorporation method, Xiao et al. used AuNR-coated DNA duplex (24-base pair (CGA)8/(TCG)8) as a drug-loading scaffold. DNA-AuNRs were further conjugated with NH_2-terminated PEG-folic acid. AuNR-conjugated capture strands (ONT-NR) were treated with targeting

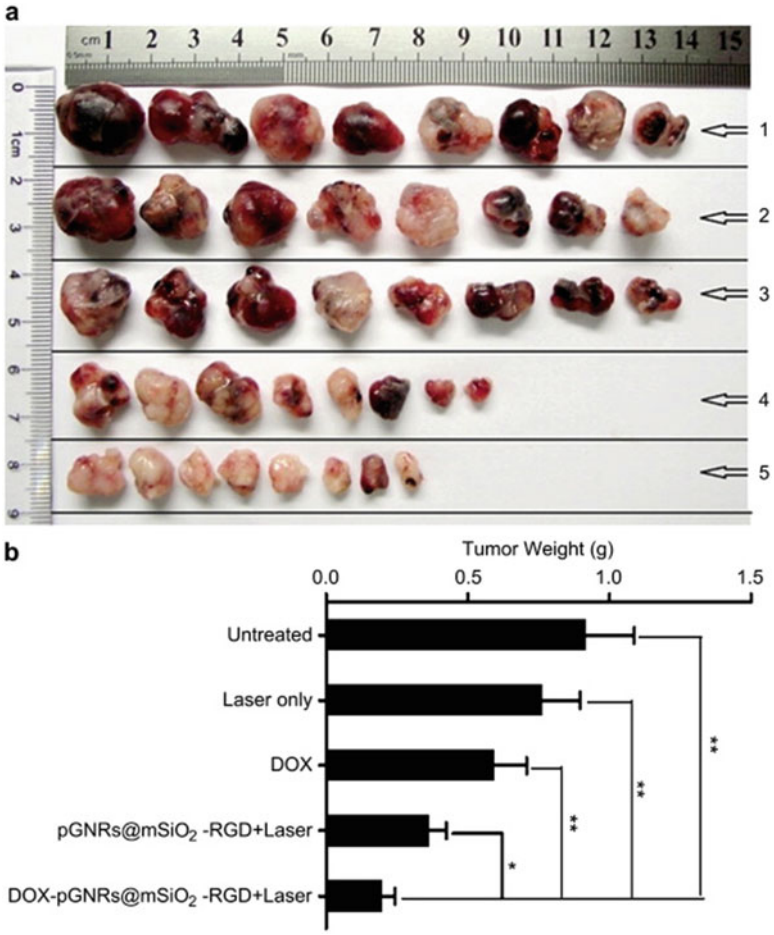

Fig. 10.5 (**a**) Photograph of tumors after excision from (1) untreated group, (2) laser group, (3) DOX group, (4) pGNRs@$mSiO_2$-RGD with laser group, and (5) DOX-pGNRs@$mSiO_2$-RGD with laser group. (**b**) Tumor weights of each group (Reprinted by permission from American Association for Cancer Research [Biomaterials] 34, 3150–3158, Copyright 2013)

strands and DNA, which led to assembling of the targeted DNA on AuNRs (T-DNA-NR). Human nasopharyngeal epidermoid carcinoma (KB) cells were used for in vivo studies. KB cells are overexpressed with folate receptors. The in vitro and in vivo results proved that T-DNA-NR delivered the anticancer drugs to the targeted cells upon NIR irradiation [20]. Regardless of methods that have been used for chemotherapy and PTT using AuNR nanomaterials as a source and which provide a highly effective suppression of cancer cell growth due to their good NIR light penetration, there are no changes in morphology, good heat capability, etc.; SiO_2-coated AuNRs also improved the drug release rate, because of their good dispersion

and ultrasmall pore size. In the upcoming years, researchers need to concentrate to prepare second or third NIR biological window sensitive AuNRs, similar to Tsai et al. reported rod-in-shell AuNRs [47].

10.2.3 Gold Nanocages for PTT and Chemotherapy Applications

Gold nanocages (AuNCGs) are a promising material in gold nanostructure, which are attractive in therapeutic applications. Generally AuNCGs localized surface plasmon resonance (LSPR) peaks observed from 600 to 1200 nm, and it can be controllable by changing the size and wall thickness of AuNCGs. For the first time, AuNCGs were used for PTT by Xia and co-workers. The AuNCG edge length was found to be 65 $\pm$ 7 nm by TEM and exhibited a strong absorption peak at 800 nm. This was conjugated with monoclonal antibodies (antiHER2) for target of breast cancer cells (SK-BR-3). The PTT effect was enumerated using flow cytometry. After the irradiation of NIR laser, the antiHER2-AuNCGs killed the cancer cells [55]. The same research group developed the method for drug delivery system with AuNCGs, and it was coated with thermosensitive polymers of poly-(N-isopropylacrylamide) (pNIPAAm). This polymer was adsorbed on the surface of AuNCGs. The pNIPAAm-AuNCGs have shown that the edge thickness was ~3 nm and the edge thickness of pNIPAAm-AuNCGs was increased to ~5 nm at 37 °C and shrank again to ~3 nm on heating to 41 °C. This temperature-based reversible size changes were applied for the pre-loaded effector to the controlled release of drugs with the help of NIR laser irradiation [56].

Shi et al. have developed AuNCGs conjugated with calcium phosphate-coated magnetic nanoparticles (Fe_3O_4@CaP-AuNCGs) for controlled release of DOX. The DOX release and cancer cell killing efficacy are higher in combined PTT-chemotherapy than the AuNCG-induced PTT without DOX (Fig. 10.6). Further, the magnetic compound was used as MRI contrast agent for target-specific drug delivery [57].

In addition, the hollow-structured Au nanocage was developed by Xia et al. with galvanic replacement technique. During the titration of 30 nm Ag nanocubes with different volume of $HAuCl_4$ solution, they have observed the absorbance shifting from visible to NIR region. Finally they optimized that a 45 nm size of (3.5 nm wall thicknesses) Au nanocubes have shown the absorbance at 810 nm. The PTT studies were performed with SK-BR-3 human breast cancer, and this is overexpressed in the EGFR. The PEG-coated anti-EGFR-AuNCs was treated with SK-BR-3, and it was irradiated with 810 nm pulse laser with a power density of 1.5 W/cm^2 for 5 min. For imaging, the cells were treated with calcein AM and ethidium homodimer 1 (EthD-1) and examined by fluorescence microscopy. Calcein AM is non-fluorescent, but because of enzymatic reaction, living cells can convert into fluorescent green calcein. But, EthD-1 is red fluorescent compound, and it can

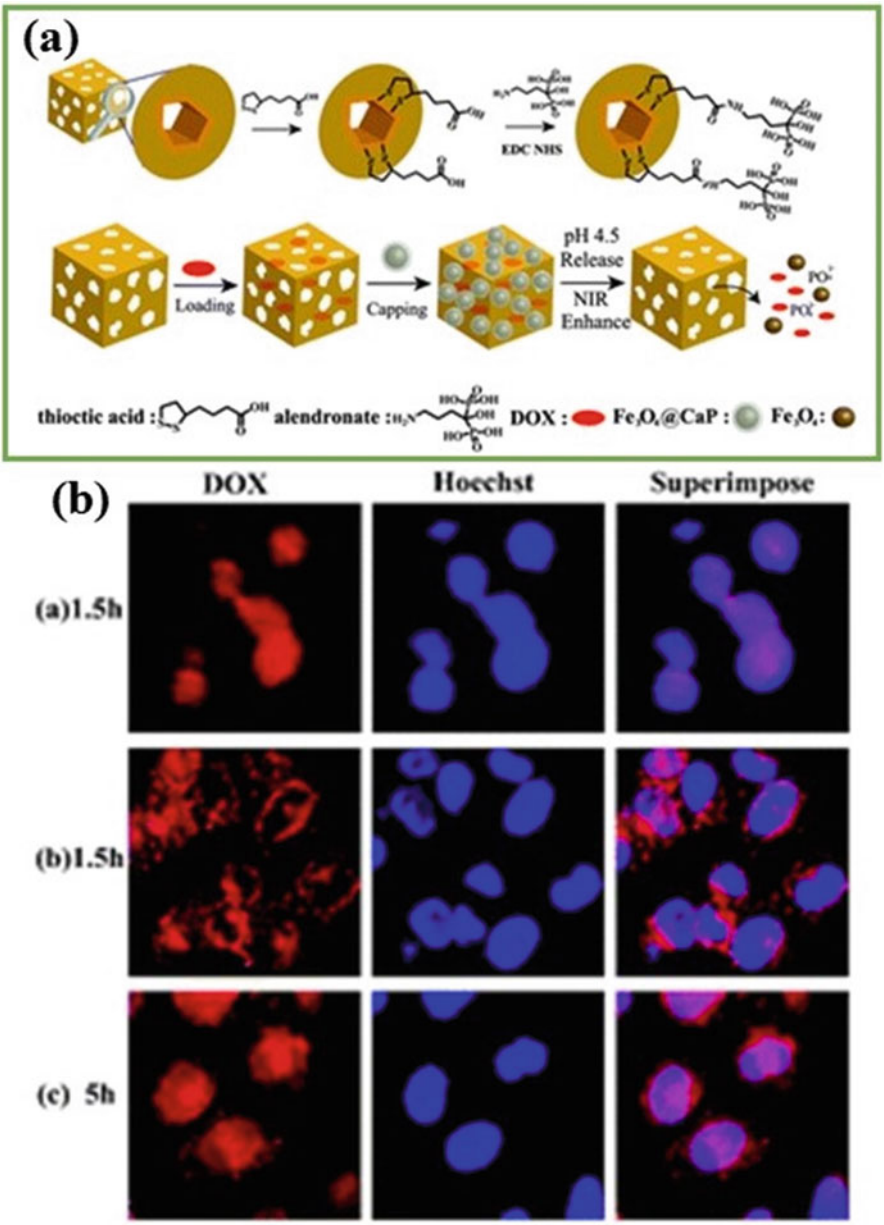

Fig. 10.6 (**a**) Schematic illustration of the preparation of Fe_3O_4@CaP capped AuNCs. Fluorescence microscopy images of live MCF-7 cells treated with Hoechst, free DOX, and AuNCs-DOX (DOX = 1.65 μg mL^{-1}). (**a**) Free DOX for 1.5 h exposure, (**b**) AuNCs-DOX for 1.5 h exposure, (**c**) AuNCs-DOX for 5 h exposure (blue fluorescence is associated with Hoechst; the red fluorescence is expressed by free DOX, released DOX, and DOX retained within Fe_3O_4@CaP capped AuNCs) (Reprinted by permission from The Royal Society of Chemistry [Chemical Communication] 48, 7640–7642 Copyright 2012)

easily penetrate through cell walls and nucleus membranes to stain DNAs, and it can indicate the cellular death. From their fluorescence imaging results, the live cells are stained and produced green fluorescence, but black is dead cells [58].

Ke et al. have developed the gold-nanoshelled microcapsules (MC-AuNS) by electrostatic interaction with gold nanoparticles and polymeric microcapsules, and the AuNS was developed by surface seeding method. The polymeric microcapsule was prepared by PLA and polyvinyl alcohol (PVA) through the water-in-oil-in-water double-emulsion method [59], and showed a zeta potential of −25 mV. While they have coated the positively charged poly(allylamine hydrochloride) (PAH), the zeta potential was found to be +2 mV. This positive charge surface was used to electrostatically adsorb negatively charged citrate-capped gold nanoseeds to nucleate the growth of a gold on microcapsule surface. The resultant microcapsule-coated AuNS (MC-AuNS) having the contrast agent ability for ultrasound imaging. In PTT, the MC-AuNS was treated with HeLa cells and was irradiated with 808 nm laser with a power intensity of 8 W/cm^2. The cell viability of HeLa cells was found to be 20% after the irradiation, and the cell demolition was observed by fluorescence imaging [60]. Further, a gold tetrahedral nanocage (AuTNC) was developed by Qian. AuTNC was prepared by galvanic replacement of AgTNC using $HAuCl_4$ solution, and it exhibited the absorption at 850 nm. A549 and SK-BR-3 cancer cells were treated with AuTNCs for 3 h, and subsequently 808 nm laser irradiated with a power density of 2 W/cm^2 for PTT study. It was found that after irradiation of NIR laser, the apparent cell deaths were observed, whereas in the absence of AgTNCs, treated cells were not dead. This confirmed that the AuTNCs are an effective material for the PTT [61].

In this work, Huang reported the synthesis of anti-miR-181b antibody coated with polyethyleneimine (PEI)-modified and folate receptor (FR)-targeted PEGylated gold nanocages (PTP-AuNCs) for PTT. First AuNCs surface was modified with SH-PEG-folic acid and followed by the conjugation with PEI, and then antibody was coated by electrostatic interactions. The in vivo and in vitro experiments of PTP-AuNCs have shown the higher efficiency to kill the cancer cells after the irradiation with NIR laser [62]. Further, a nanocage with less than 45 nm in length and wall thickness of 3.5 nm was prepared by Chen et al., and it showed a strong resonance absorption peak at 810 nm. SK-BR-3 breast cancer cell line, which overexpresses the EGFR2 or HER2, has been used for the PTT applications. For active targeting, the nanocages are coated with PEG and antiHER2; the resultant nanocages exhibited an absorption band at 812 nm. For PTT study, the cancer cells are treated with antibody-coated nanocages, and it was allowed to pass the pulse laser with 810 nm. Here also calcein and EthD-1 staining are used for the imaging studies and found that the red fluorescence region corresponds nicely to the void region in the green calcein fluorescence image. This is confirming the cancer cell death after the irradiation of NIR laser. In control experiments, cells in the absence of antibody-coated gold nanocages have shown no noticeable loss of viability [63].

The AuNC-based in vivo PTT studies were performed by the same research group. PEG-coated nanocages were treated with U87wtEGFR human glioblastoma

cells, and 808 nm laser was irradiated with a power density of 0.5 W/cm^2 to perform PTT. The PEG-AuNCs supported the accumulation in the cancer cells for 72 h postinjection. After the PTT, the metabolic changes are studied with F-fluorodeoxyglucose (F-FDG) positron emission tomography imaging. Generally the dead cells will not uptake the F-FDG (no metabolic activity), and this is useful to predict the dead cell level by imaging studies. After the NIR laser irradiation, a 70% reduction in metabolic activity has been shown, with the comparison to those without irradiation. The histological photographs of laser-irradiated tumors from mice treated with nanocages have shown the cellular damage in abundant pyknosis, karyorrhexis, karyolysis and interstitial edema. These characterizations were absent without PEG-coated nanocages [64]. AuNCGs are a novel material for photothermal therapeutic applications. In particular, AuNCG NIR absorption cross section is five orders higher than the conventional organic dye of indocyanine green (ICG), and their controllable size also can expedite for drug delivery applications. In addition, mesoporous silica-coated AuNCGs and porous-structured AuNCGs also substitute material for encapsulation and control release of anticancer drugs with combined chemophotothermal therapy.

10.2.4 Hollow Gold Nanospheres for PTT and Chemotherapy Applications

The HAuNSs can be classified into three types based on their drug loading such as (1) loaded inside the hollow interior of HAuNSs [65], (2) conjugated to the surface of HAuNSs [8], and (3) co-loaded to soft matrix, such as polymeric microspheres or liposomes [66, 67]. The HAuNSs are ideal for chemo and PTT. Because of their smaller size ($d = 40$ nm), the mammalian cell intracellular uptake is higher and has better extravasation from tumor blood vessels. You et al. reported a PLGA-coated HAuNS-based PTT-containing paclitaxel (PTX), and showed the LSPR peak around 800 nm. For in vitro study, PTX-PLGA-HAuNSs are incubated with human U87 gliomas and MDA-MB-231 mammary tumor cells. The drug release was monitored with PLGA-HAuNSs under 808 nm laser irradiation. The hypothetical structure of microspheres of PLGA-HAuNSs was prepared by a water-in-oil-in-water (W1/O/W2) double-emulsion solvent evaporation method. PTX was dissolved in organic phase with PLGA, whereas HAuNSs was dissolved in aqueous solution. After the irradiation with 808 nm laser, cancer cells were killed by the released PTX [66]. Further, Liang et al. have developed the method for the PTT using anti-cMet antibody-conjugated hollow gold nanospheres (A-HAuNS). The A-HAuNS was treated with HeLa and CaSki epidermoid cervical carcinoma cells, and then it was irradiated with NIR laser. The apoptotic rates of HeLa and CaSki were found to be 5.83% and 20.0%, respectively. The A-HAuNS has a capability of specific elimination of cancer cells by PTT [68].

The hollow HAuNSs (∼40-nm diameter) was used for PTT and DOX release upon NIR laser irradiation. 63% DOX was loaded to PEG-coated HAuNSs. Irradiation with NIR laser induced photothermal conversion, which triggered rapid DOX release from DOX-loaded HAuNSs. The DOX-loaded HAuNSs was treated with MDA-MB-231 cells, and increased amount of cancer cells were killed under NIR laser irradiation [69]. In another work, PEG-coated HAuNSs were used for DOX release. The anticancer activity of DOX@PEG-HAuNSs was studied by the irradiation of NIR laser, in vitro and in vivo using human MDA-MB-231 breast cancer and A2780 ovarian cancer cells. The DOX@PEG-HAuNSs-plus-NIR laser confirmed the greater anticancer activity than free DOX. By using DOX@PEG-HAuNSs as a single agent for chemophotothermal therapy, it demonstrated itself one of the best approaches for anticancer therapy [70].

Melancon et al. reported the NIR light-irradiated anti-EGFR monoclonal antibody C225 conjugated with HAuNSs (C225-HAuNSs). After the irradiation of NIR laser with a power density of 4 W/cm^2 for 3 min, the maximum temperature was 65.2 ± 0.10 °C in A431 tumor xenograft of mice treated with C225-HAuNSs. More than twofold increase of DTPA-Gd was found, by MRI activity, in mice injected with C225-HAuNSs under NIR laser irradiation. From dynamic contrast-enhanced MRI, more twofold increase of the polymeric drug was found in mice injected with C225-HAuNSs under NIR laser irradiation, compared with the control mice. Optical imaging study confirmed that the tumor uptake of polymeric drug was higher in mice after the NIR laser irradiation [71]. Greater absorption efficiency, optical tenability, and lesser damage of nanomaterials, which lead to be a HAuNSs, are promising materials for PTT. However, some unresolved issues remain to be addressed, such as acquisition of a better understanding of the interaction between HAuNSs and cancer cells. While there has been some progress made for the synthesis of second biological NIR window absorptive HAuNSs, further research is clearly needed to prepare third and fourth biological NIR window absorptive HAuNSs to improve the photothermal efficiency.

10.2.5 Gold Nanostars for PTT and Chemotherapy Applications

The gold nanostars (AuSrs) usually show the LSPR broad NIR-absorptive peaks. The anisotropic and multiple sharp pinpoint shapes of AuSrs can enhance the effect of thermal transduction under the irradiation of NIR laser. The AuSrs showed the superior biocompatibility than AuNRs and AuNCGs and easy to synthesis. The AuSrs can enhance the drug-loading percentage, because of their star shape and frequently used for PTT. TAT-peptide-AuSrs were demonstrated superior than PEG-AuSrs to enter into cancer cells. BT549 breast cancer cells were killed by TAT-AuSrs under NIR laser irradiation of 0.2 W/cm^2. Real-time live-cell TPL established that the uptake of TAT-AuSrs tangled actin-driven lipid-raft-mediated macropinocy-

tosis. These results confirmed that the AuSrs are a promising theranostic agent for cancer therapy [72]. Wang et al. attached the chlorine 6 (Ce6) on the surface of AuSrs and used for PTT. AuSrs-Ce6 exhibited an absorption peak in NIR region, and PTT and photodynamic therapy (PDT) are induced under NIR irradiation. The MDA-MB-435 breast cancer cells and A549 lung cancer cells are treated with PEG-coated AuSrs-Ce6 (PEG-AuSrs-Ce6). Under the irradiation of 671 nm laser, PTT efficacy was enhanced in PEG-AuSrs-Ce6, but not in Ce6 due to photobleaching of Ce6. The higher cellular uptake of PEG-AuSrs-Ce6 was found. This is the first report for combined PDT and PTT based on PEG-AuSrs-Ce6 [73].

Shi and co-workers reported a Fe_3O_4@Au@hyaluronic acid-nanostars (Fe_3O_4@Au-HASrs) for magnetic resonance (MR), computed tomography (CT), and PT therapies. First, Fe_3O_4@Ag seeds were prepared by one-pot hydrothermal method. The aqueous $FeCl_2$ was mixed with ammonium hydroxide; after 10 min of vigorous stirring, the mixture was transferred into autoclave, and SH-PEG-coated AgNPs was added into autoclave solution. Then, the solution was heated to 134 °C for 3 h. After autoclave cooled to room temperature, the resultant solution was purified by magnetic separation. The separated Fe_3O_4@Ag seeds were further purified three times by rinsing with water. $HAuCl_4$, CTAB, $AgNO_3$, and ascorbic acid were added into a beaker and vigorously stirred for 10 min, and then 0.1 mL of Fe_3O_4@Ag seed solution was mixed. The color of the solution was changed to blue within a few min. The stirring was continued to 1 h, and then the particles were purified by centrifugation. The SH-PEI was coated on Fe_3O_4@AuSrs and finally using EDC and NHS chemistry, and HA was coated on Fe_3O_4@AuSrs, and the resultant Fe_3O_4@Au-HASrs was purified by centrifugation. The obtained Fe_3O_4@Au-HASrs exhibits the absorption band at 870 nm. The mean diameter of the internal AuSrs was reported to be 119.4 ± 19.4 nm. Apart from the PTT, they have used this material for in vivo and in vitro MR and CT imaging applications. For PTT, Fe_3O_4@Au-HASrs was irradiated with 915 nm laser with a power density of 1.2 W/cm^2. 24 mM Au concentration of Fe_3O_4@Au-HASrs has shown that the temperature increases to 81.2 °C after 300 s irradiation of laser, whereas, Fe_3O_4@Ag seeds do not show the noticeable temperature changes. HeLa cells were used for in vitro and in vivo PT ablation. In vitro studies show that Fe_3O_4@Au-HASrs killed 62.2% of HeLa cells under the irradiation time of 10 min. HeLa cell-bearing mice were injected with PBS containing 32 mM Au concentration of Fe_3O_4@Au-HASrs. It was observed that mice treated with Fe_3O_4@Au-HASrs under 915 nm laser irradiation show a 100% survival rate after 60 days, whereas the mice without treatment, only laser treatment, and treated with only Fe_3O_4@Au-HASrs are 25%, 0%, and 0%, respectively. The obtained in vivo and in vitro data suggest that the Fe_3O_4@Au-HASrs has a promising material for the PTT of tumors [74].

The multifunctional AuSrs were prepared by Wang et al. and applied them for the tumor therapeutic applications. The AuSrs were coated with SH-PEI and SH-PEG, and then folic acid also was coated on the surface of AuSrs; the

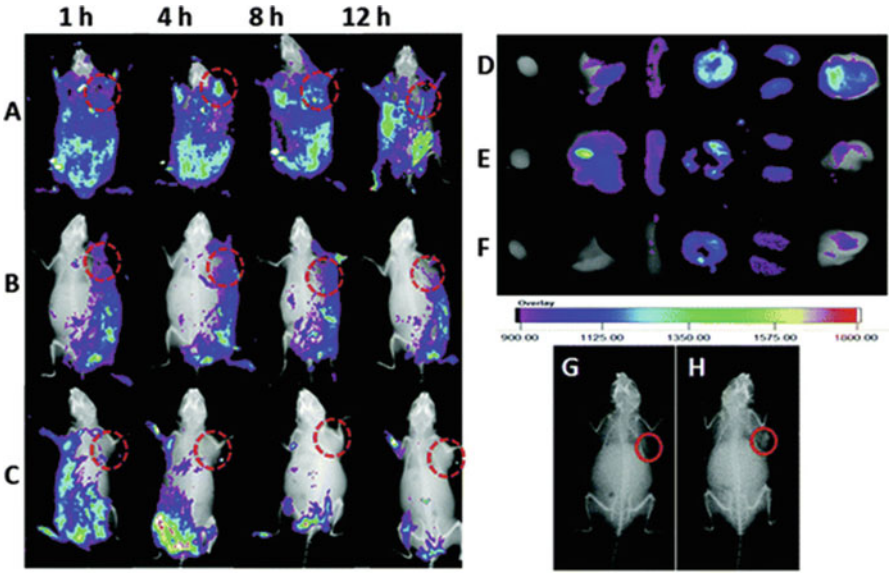

Fig. 10.7 In vivo and ex vivo NIR fluorescence and X-ray imaging. Representative in vivo fluorescence images of tumor-bearing mice following tail vein administration of (**a**) GNSTs-PEG/PEI-FA/Cy5.5, (**b**) GNSTs-PEG/PEI/Cy5.5, and (**c**) free Cy5.5 at different time points. Ex vivo NIR fluorescence images of major organs and tumors dissected from mice at 12 h after injection of (**d**) GNSTs-PEG/PEI-FA/Cy5.5, (**e**) GNSTs-PEG/PEI/Cy5.5, and (**f**) free Cy5.5. In vivo X-ray imaging of (**g**) control (26 HU) and (**h**) the DOX/GNSTs-PEG/PEI-FA-treated group (72 HU) [75] (Reprinted by permission from The Royal Society of Chemistry [J. Mater. Chem. B] 4, 5895–5906, Copyright 2016)

resultant PEG@PEI-FA@AuSrs show the particle size 148.2 ± 3.2 nm, which was measured by TEM; and the zeta potential was found to be 14.5 ± 1.2 mV. The HeLa cell uptake of DOX was detected by flow cytometry. After 4 h incubation of HeLa cells with DOX@PEG@PEI-FA@AuSrs, it was noted that the cell nuclei were labeled with DAPI. Further, they have reported that FA-targeted DOX@PEG@PEI@AuSrs have shown the nuclei red fluorescence more intense than nontargeted DOX@PEG@PEI@AuSrs. For in vivo studies, NIR thermal camera was used to predict the temperature changes under radiofrequency irradiation treatment. The temperature was increased to 43.7 °C within 5 min radiofrequency irradiation, with after 4 h injection of DOX@PEG@PEI–FA@AuSrs. The obtained lower heat did not affect the normal skin and blood circulation (Fig. 10.7). The in vitro and in vivo studies confirmed that DOX@PEG@PEI–FA@AuSrs can effectively kill the cancer cells through their pH-sensitive and controlled release of DOX with radiofrequency thermal therapy [75]. To maximize the photothermal therapeutic efficiency of AuSrs, delicate and versatile surface modifications are still highly desirable.

10.2.6 Gold Nanocluster for Bioimaging and Drug Delivery Applications

The fluorescence of AuNCs highly depends on their size, shape, and solvent medium. AuNCs has shown extreme surface coverage, which will make them a suitable candidate for the drug delivery and bioimaging applications. The orange-red emittive pentapeptide-capped AuNCs (ppt-AuNCs) was synthesized by simple mixing with $HAuCl_4$ and pentapeptide, and then it was heated at 80 °C for 17 h. The ppt-AuNCs shows the emission maximum at 606 nm with an excitation wavelength of 360 nm, and the particle size was found to be 1.76 nm by TEM. The quantum yield of ppt-AuNCs was calculated to be 1.8%. ppt-AuNCs was applied for tumor targeting and bioimaging and due to their zwitterionic nature. It was accumulated more in cancer cells, and their smaller size also facilitates the urinary excretion, and it reaches nearly 82% after 24 h injection [76].

Lakshmi et al. prepared four different sizes of gold nanocluster by etching of gold nanoparticles with GSH ligand. First gold nanoparticles were synthesized by using mercaptosuccinic acid (MSA) ligand, and it was mixed with $HAuCl_4$ in methanol medium, and then $NaBH_4$ was added at 0 °C. The obtained MSA-AuNPs was used as starting materials to synthesize different sized and fluorescent AuNCs. AuNCs1 was prepared by mixing of MSA-AuNPs and GSH, and then pH was adjusted to 1.5; this solution was stirred to 12 h in room temperature. AuNCs2 was synthesized by mixing of MSA-AuNPs and GSH at room temperature, and the reaction was continued to 12 h at 70 °C. AuNCs3 was prepared by mixing of MSA-AuNPs and GSH at 0 °C, and then reaction was continued for 12 h at 70 °C. AuNCs4 was synthesized by mixing of MSA-AuNPs and GSH at room temperature, and the pH was adjusted to 10, and the reaction was allowed to complete to 12 h at 70 °C. The particle size was found to be from 0.7 to 2 nm, and the quantum yield was calculated to be 0.85, 2.5, and 24% of AuNCs1, AuNCs2, and AuNCs3, respectively. The emission maximum was observed around 530 and 750 nm for AuNCs1, AuNCs2, and AuNCs3, whereas AuNCs4 exhibits the emission maximum at 412 nm. These results revealed that the reaction conditions such as temperature and pH are the major role for the formation of AuNCs by etching method. These AuNCs were applied for bioimaging and urea sensor applications [77].

The BSA-AuNCs-coated cisplatin prodrug was developed and used for the bioimaging and targeted therapy of breast cancer. The folic acid was also covalently attached with BSA-AuNCs-coated cisplatin prodrug (FA-BSA-AuNCs-Pt), and it induced the cellular apoptosis through intracellular activation of the cisplatin prodrug. In vitro study showed that the FA-BSA-AuNCs-Pt inhibits the growth of breast cancer cells [78]. Further, mesoporous silica core of BSA-AuNCs (MSN@AuNCs) was developed by Jonas et al. and applied for dual-drug delivery. BSA-AuNCs and MSN@AuNCs are separately synthesized. The negatively charged gemcitabine (GEM) drug was loaded in positively charged MSN, positively charged DOX drug

was loaded into negatively charged BSA-AuNCs, then drug-loaded nanomaterials were mixed together, and they electrostatically attached together. The pH-sensitive MSN@AuNCs nanomaterial will release the dual drugs after reaching to the cancer cells due to low-pH environment. Further, it was performed with in vitro tumor imaging (Fig. 10.8) [79].

Eggs are commonly used as a protein source to prepare AuNCs. Linlin et al. prepared the egg white, egg yolk, fetal bovine serum, mouse serum, and human serum-capped AuNCs, and it exhibits an emission maximum at 635 nm (λ_{ex}: 489 nm), 654 nm (λ_{ex}: 490 nm), 633 nm (λ_{ex}: 488 nm), 663 nm (λ_{ex}: 487 nm), and 660 nm (λ_{ex}: 487 nm), respectively. The average particle size was found to be 2.4 nm, and the quantum yields of white yolk-AuNCs and FBS-AuNCs were found to be 3.3 and 2.4%. These AuNCs were utilized for bioimaging applications. Nearly 100% of the HepG2 cells showed red emission in nuclei and cytoplasm area (Fig. 10.9) [80].

Histidine and SH-PEG-AuNCs (H@PEG-AuNCs) were used for drug delivery applications. H@PEG-AuNCs shows the emission maximum at 575 nm with an excitation wavelength of 261 nm. The particle size was found to be 1.5–1.8 nm, and the quantum yield was calculated to be 1.3–1.8%. H@PEG-AuNCs was used for the delivery of DOX, and it has shown the negligible toxicity to A549 lung cancer cells [81]. In addition, glutathione-capped Au/Ce-AuNCs (GSH-Au/Ce-AuNCs) exhibits a dual emission at 570 and 360 nm, while excite at 290 nm. Yellow-orange fluorescence was observed under UV light, and the particle size was found to be 1.2–2.2 nm. It was applied for in vivo tumor targeting and bioimaging applications. It was noted that 25–350 μM concentration of GSH-Au/Ce-AuNCs has no obvious cell cytotoxicity effect on HeLa, HepG2, and L02 cells. Further, normal cells have no noticeable absorption of GSH-Au/Ce-AuNCs [82]. In addition to the Au/Ce-AuNCs, green emittive 1-methyl-3-propylimidazolium bromide capped AuNCs (MPB-AuNCs) was synthesized by Shyamtanu et al., and it displays the emission maximum at 510 nm, with an excitation wavelength of 405 nm. The particle size was found to be 1–2 nm. It was used for the bioimaging of three types of human cancer cells such as lung (A549), breast (MCF-7), and colon (HCT116) by confocal microscopy. The cytotoxicity studies confirmed that the MPB-AuNCs are nontoxic for both cancer and normal cells [83]. Generally, AuNCs emissions are tunable from the UV to NIR region. NIR-emittive AuNCs has been extensively applied for bioimaging, which enhanced transparency of biological tissues and rise the biocompatibility. The existing AuNCs have some drawbacks such as moderate lifetime and also modest excitation efficiency in NIR regions. To improve these drawbacks, long-lived fluorescent AuNCs are needed, and it can increase the contrast by the way of minimizing tissue autofluorescence and background scattering.

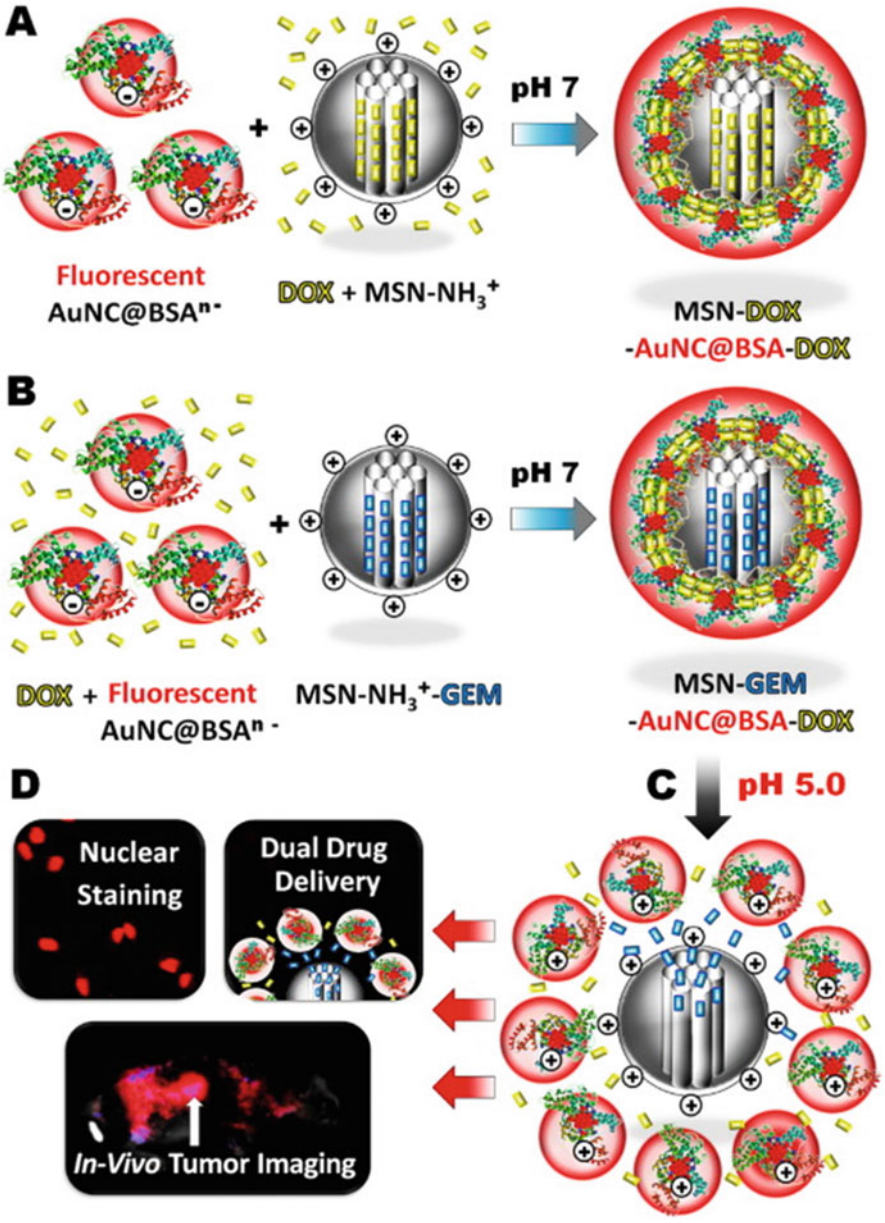

Fig. 10.8 Self-assembly of fluorescent negatively charged AuNC@BSA with positively charged DOX-loaded MSN-NH_3^+ leading to DOX-loaded MSN-AuNC@BSA carrier (**a**). Self-assembly of fluorescent negatively charged AuNC@BSA and DOX with positively charged GEM-loaded MSN-NH_3^+ leading to MSN-AuNC@BSA carrier loaded with two drugs (**b**), which could be disrupted by an acidic pH trigger (**c**). Applications of multifunctional dual-drug-loaded MSN-AuNC@BSA nanocarriers (**d**) [79] (Reprinted by permission from Elsevier [Journal of Controlled Release] 229, 183–191, Copyright 2016)

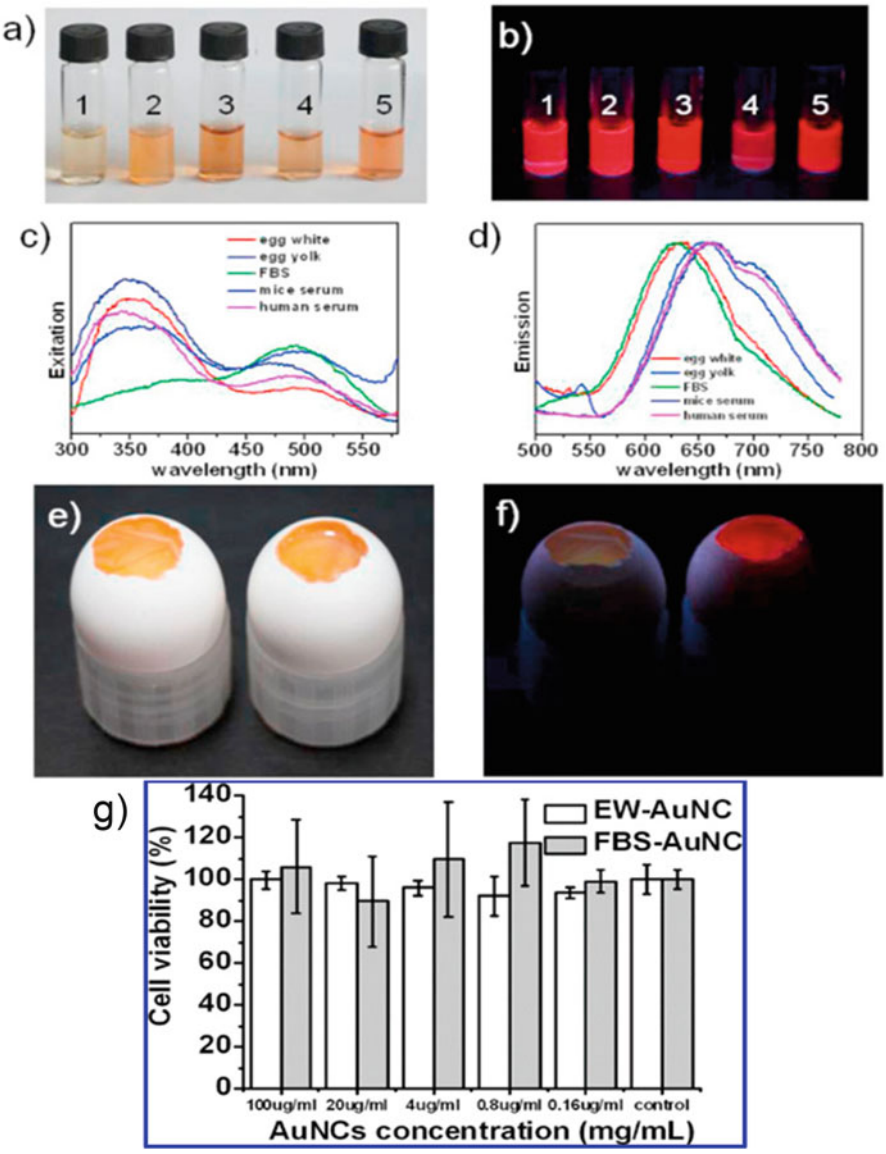

Fig. 10.9 Photographs of biosynthesized gold nanoclusters with red fluorescence protected by (1) egg white (EW), (2) egg yolk (EY), (3) fetal calf serum (FBS), (4) mouse serum, and (5) human serum in water under (**a**) visible and (**b**) UV light (365 nm). (**c**) Photoluminescence excitation spectra (PLE) and (**d**) photoluminescence spectra (PL) of the gold nanoclusters. For the PLE spectra, a fixed emission at 600 nm was used. For the PL spectra, excitation at 470 nm was used. Photographs of chicken eggs without treatment (*left*) and with biosynthesized gold nanoclusters (*right*) under (**e**) visible and (**f**) UV light ($\lambda_{ex} = 365$ nm). (**g**) Cell viability of HepG2 cells treated with EW-AuNCs and FBS-AuNCs by WST-1 assays. HepG2 cells were incubated with the AuNCs of different concentrations for 24 h, and then cell viability was detected [80] (Reprinted by permission from Elsevier [Optics Communications] 355, 567–574, Copyright 2015)

10.3 Conclusions and Trends

The gold nanomaterials are extensively used in the field of drug delivery. In particular, heat can be generated by NIR-sensitive gold nanomaterials under NIR laser irradiation. Local heat can be transduced by photons of irradiation, and this PTT heat efficiency induced the drug release through the chemotherapy. It is known that the NIR-sensitive gold nanomaterial-based cancer therapy has been proven to higher efficacy of cancer cell death by both in vivo and in vitro experiments.

In this book chapter, we have discussed the significance of NIR-sensitive gold nanomaterials and their PTT and chemotherapeutic applications. In the future, the following consideration is an essential to improve this field: (1) instead of laser irradiation, it is a better choice to use fiber-optic technologies or nano-optical heating methods to improve the drug release percentage to more cancer cells, (2) NIR-sensitive Au nanomaterials combined with graphene material therapy of PTT and chemotherapy can induce the rate of drug loading and releasing and further induce the thermosensitive response, and (3) to develop the in situ photothermolysis method [84] and (4) the use of dual NIR-sensitive materials such as AuNRs and Ce6, AuNRs with up-conversion nanomaterials can induce the PTT efficiency and to select the second biological window nanomaterial (higher than 900 nm) irradiation for deeper penetration to the cells. Furthermore, aggregation of nanomaterials and vapor evolution occur during laser irradiation, and it is detrimental to normal cells; these should be overcome before developing nanomaterials for PTT and chemotherapy [84]. In addition, nanomaterials can be demolished by the use of high power density of laser irradiation [85–87]. Considering these suggestions, a promising nanomaterial with high sensitivity and cost-effectiveness can be constructed for cancer treatment.

References

1. http://www.who.int/mediacentre/factsheets/fs297/en/
2. https://www.cancer.org/
3. Z. Zhang, J. Wang, C. Chen, Near-infrared light-mediated nanoplatforms for cancer thermochemotherapy and optical imaging. Adv. Mater. **25**, 3869–3880 (2013)
4. R. Guo, L. Zhang, H. Qian, R. Li, X. Jiang, B. Liu, Multifunctional nanocarriers for cell imaging, drug delivery, and near-IR photothermal therapy. Langmuir **26**(8), 5428–5434 (2010)
5. V. Shanmugam, S. Selvakumar, C.-S. Yeh, Near-infrared light-responsive nanomaterials in cancer therapeutics. Chem. Soc. Rev. **43**, 6254–6287 (2014)
6. X. Huang, I.H. El-Sayed, W. Qian, M.A. El-Sayed, Cancer cell imaging and photothermal therapy in the near-infrared region by using gold nanorods. J. Am. Chem. Soc. **128**, 2115–2120 (2006)
7. A.M. Smith, M.C. Mancini, S. Nie, Bioimaging: Second window for in vivo imaging. Nat. Nanotechnol. **4**, 710–711 (2009)
8. C.M. Cobley, J. Chen, E.C. Cho, L.V. Wang, Y. Xia, Gold nanostructures: A class of multifunctional materials for biomedical applications. Chem. Soc. Rev. **40**, 44–56 (2011)

9. A. Llevot, D. Astruc, Applications of vectorized gold nanoparticles to the diagnosis and therapy of cancer. Chem. Soc. Rev. **41**, 242–257 (2012)
10. B.N. Khlebtsov, N.G. Khlebtsov, On the measurement of gold nanoparticle sizes by the dynamic light scattering method. Colloid J. **73**, 118–127 (2011)
11. K. Park, L.F. Drummy, R.C. Wadams, H. Koerner, D. Nepal, L. Fabris, R.A. Vaia, Growth mechanism of gold nanorods. Chem. Mater. **25**, 555–563 (2013)
12. M. Liu, P. Guyot-Sionnest, Mechanism of silver(I)-assisted growth of gold nanorods and bipyramids. J. Phys. Chem. B **109**, 22192–22200 (2005)
13. H. Wang, D.W. Brandl, F. Le, P. Nordlander, N.J. Halas, Nanorice: A hybrid plasmonic nanostructure. Nano Lett. **6**, 827–832 (2006)
14. B.N. Khlebtsov, V.A. Khanadeev, I.L. Maksimova, G.S. Terentyuk, N.G. Khlebtsov, Silver nanocubes and gold nanocages: Fabrication and optical and photothermal properties. Nanotechnol. Russ. **5**(7–8), 454–468 (2010)
15. A. Guerrero-Martínez, S. Barbosa, I. Pastoriza-Santos, L.M. Liz-Marzán, Nanostars shine bright for you: Colloidal synthesis, properties and applications of branched metallic nanoparticles. Curr. Opin. Colloid Interface Sci. **16**, 118–127 (2011)
16. F. Kim, S. Connor, H. Song, T. Kuykendall, P. Yang, Platonic gold nanocrystals. Angew. Chem. Int. Ed. **43**, 3673–3677 (2004)
17. M. Grzelczak, J. Pérez-Juste, P. Mulvaney, L.-M. Liz-Marzán, Shape control in gold nanoparticle synthesis. Chem. Soc. Rev. **37**, 1783–1791 (2008)
18. C. Burda, X. Chen, R. Narayanan, M.A. El-Sayed, Chemistry and properties of nanocrystals of different shapes. Chem. Rev. **105**(4), 1025–1102 (2005)
19. R. Bukasov, J.S. Shumaker-Parry, Highly tunable infrared extinction properties of gold nanocrescents. Nano Lett. **7**, 1113–1118 (2007)
20. Z. Xiao, C. Ji, J. Shi, E.M. Pridgen, J. Frieder, J. Wu, O.C. Farokhzad, DNA self-assembly of targeted near-infrared-responsive gold nanoparticles for cancer thermo-chemotherapy. Angew. Chem. Int. Ed. **51**, 11853–11857 (2012)
21. X. Zhang, K. Wang, M. Liu, X. Zhang, L. Tao, Y. Chen, Y. Wei, Polymeric AIE-based nanoprobes for biomedical applications: Recent advances and perspectives. Nanoscale **7**, 11486–11508 (2015)
22. D.P. O'Neal, L.R. Hirsch, N.J. Halas, J.D. Payne, J.L. West, Photo-thermal tumor ablation in mice using near infrared-absorbing nanoparticles. Cancer Lett. **209**, 171–176 (2004)
23. J.H. Breasted, *The Edwin Smith Surgical Papyrus*, vol 1 (University of Chicago, Chicago, 1930)
24. L.R. Hirsch, R.J. Stafford, J.A. Bankson, S.R. Sershen, R.E. Price, J.D. Hazle, N.J. Halas, J.L. West, Nanoshell-mediated near-infrared thermal therapy of tumors under magnetic resonance guidance. Proc. Natl. Acad. Sci. U. S. A. **100**, 13549–13554 (2003)
25. C. Loo, A. Lowery, N. Halas, J. West, R. Drezek, Immunotargeted nanoshells for integrated cancer imaging and therapy, Nano Lett. **5**(4), 709–711 (2005)
26. A.M. Gobin, M.H. Lee, N.J. Halas, W.D. James, R.A. Drezek, J.L. West, Near-infrared resonant nanoshells for combined optical imaging and photothermal cancer therapy. Nano Lett. **7**, 1929–1934 (2007)
27. U.S. Chung, J.-H. Kim, B. Kim, E. Kim, W.-D. Jang, W.-G. Koh, Dendrimer porphyrin-coated gold nanoshells for the synergistic combination of photodynamic and photothermal therapy. Chem. Commun. **52**, 1258–1261 (2016)
28. L. Luo, Y. Bian, Y. Liu, X. Zhang, M. Wang, S. Xing, L. Li, D. Gao, Combined near infrared photothermal therapy and chemotherapy using gold nanoshells coated liposomes to enhance antitumor effect. Small **12**(30), 4103–4112 (2016)
29. D. Chen, L.L. Li, F.Q. Tang, S. Qi, Facile and scalable synthesis of tailored silica "Nanorattle" structures. Adv. Mater. **21**, 3804–3807 (2009)
30. H. Liu, D. Chen, L. Li, T. Liu, L. Tan, X. Wu, F. Tang, Multifunctional gold nanoshells on silica nanorattles: A platform for the combination of photothermal therapy and chemotherapy with low systemic toxicity. Angew. Chem. Int. Ed. **50**, 891–895 (2011)

31. H. Liu, T. Liu, X. Wu, L. Li, L. Tan, D. Chen, F. Tang, Targeting gold nanoshells on silica nanorattles: A drug cocktail to fight breast tumors via a single irradiation with near-infrared laser light. Adv. Mater. **24**, 755–761 (2012)
32. C. Wu, C. Yu, M. Chu, A gold nanoshell with a silica inner shell synthesized using liposome templates for doxorubicin loading and near-infrared photothermal therapy. Int. J. Nanomedicine **6**, 807–813 (2011)
33. S.M. Lee, H. Park, K.H. Yoo, Synergistic cancer therapeutic effects of locally delivered drug and heat using multifunctional nanoparticles. Adv. Mater. **22**, 4049–4053 (2010)
34. M.-R. Choi, K.J.S. Maxey, J.K. Stanley, C.S. Levin, R. Bardhan, D. Akin, S. Badve, J. Sturgis, J.P. Robinson, R. Bashir, N.J. Halas, S.E. Clare, A cellular trojan horse for delivery of therapeutic nanoparticles into tumors. Nano Lett. **7**, 3759–3765 (2007)
35. Y. Wang, X. Teng, J.-S. Wang, H. Yang, Solvent-free atom transfer radical polymerization in the synthesis of Fe_2O_3@polystyrene Core−Shell nanoparticles. Nano Lett. **3**, 789–793 (2003)
36. J. Kim, S. Park, J.E. Lee, S.M. Jin, J.H. Lee, I.S. Lee, I. Yang, J.-S. Kim, S.K. Kim, M.-H. Cho, T. Hyeon, Designed fabrication of multifunctional magnetic gold nanoshells and their application to magnetic resonance imaging and photothermal therapy. Angew. Chem. Int. Ed. **45**, 7754–7758 (2006)
37. X. Ji, R. Shao, A.M. Elliott, R.J. Stafford, E.E. Coss, J.A. Bankson, G. Liang, Z.-P. Luo, K. Park, J.T. Markert, C. Li, Bifunctional gold nanoshells with a superparamagnetic iron oxide-silica core suitable for both mr imaging and photothermal therapy. J. Phys. Chem. C. Nanomater. Interfaces **111**, 6245–6251 (2007)
38. Y. Su, X. Wei, F. Peng, Y. Zhong, Y. Lu, S. Su, T. Xu, S.-T. Lee, Y. He, Gold nanoparticles-decorated silicon nanowires as highly efficient near-infrared hyperthermia agents for cancer cells destruction. Nano Lett. **12**, 1845–1850 (2012)
39. R. Bardhan, W. Chen, C.P. Torres, M. Bartels, R.M. Huschka, L.L. Zhao, E. Morosan, R.G. Pautler, A. Joshi, N.J. Halas, Nanoshells with targeted simultaneous enhancement of magnetic and optical imaging and photothermal therapeutic response. Adv. Funct. Mater. **19**, 3901–3909 (2009)
40. W. Zhou, J. Shao, Q. Jin, Q. Wei, J. Tang, J. Ji, Zwitterionic phosphorylcholine as a better ligand for gold nanorods cell uptake and selective photothermal ablation of cancer cells. Chem. Commun. **46**, 1479–1481 (2010)
41. B. Nikoobakht, M.A. El-Sayed, Preparation and growth mechanism of gold nanorods (NRs) using seed-mediated growth method. Chem. Mater. **15**, 1957–1962 (2003)
42. F. Ren, S. Bhana, D.D. Norman, J. Johnson, L. Xu, D.L. Baker, A.L. Parrill, X. Huang, Gold nanorods carrying paclitaxel for photothermal-chemotherapy of cancer. Bioconjug. Chem. **24**, 376–386 (2013)
43. L. Tong, Y. Zhao, T.B. Huff, M.N. Hansen, A. Wei, J.-X. Cheng, Gold nanorods mediate tumor cell death by compromising membrane integrity. Adv. Mater. **19**, 3136–3141 (2007)
44. W. Choi, J.-Y. Kim, C. Kang, C.C. Byeon, Y.H. Kim, G. Tae, Tumor regression in vivo by photothermal therapy based on gold-nanorod-loaded, functional nanocarriers. ACS Nano **5**(3), 1995–2003 (2011)
45. C. Bremer, C.H. Tung, R. Weissleder, In vivo molecular target assessment of matrix metalloproteinase inhibition. Nat. Med. **7**, 743–748 (2001)
46. T.S. Hauck, T.L. Jennings, T. Yatsenko, J.C. Kumaradas, W.C.W. Chan, Enhancing the toxicity of cancer chemotherapeutics with gold nanorod hyperthermia. Adv. Mater. **20**, 3832–3838 (2008)
47. M.-F. Tsai, S.-H.G. Chang, F.-Y. Cheng, P.S. Vijayakumar, Y.-S. Cheng, C.-H. Su, C.-S. Yeh, Au nanorod design as light-absorber in the first and second biological near-infrared windows for in vivo photothermal therapy. ACS Nano **7**, 5330–5342 (2013)
48. G. Von Maltzahn, J.-H. Park, A. Agrawal, N.K. Bandaru, S.K. Das, M.J. Sailor, S.N. Bhatia, Computationally guided photothermal tumor therapy using long-circulating gold nanorod antennas. Cancer Res. **69**, 3892–3900 (2009)
49. X. Kang, X. Guo, W. An, X. Niu, S. Li, Z. Liu, Y. Yang, N. Wang, Q. Jiang, C. Yan, H. Wang, Q. Zhang, Photothermal therapeutic application of gold nanorods-porphyrin-trastuzumab complexes in HER2-positive breast cancer. Sci Rep **7**, 42069 (2017)

50. X. Su, B. Fu, J. Yuan, Gold nanocluster-coated gold nanorods for simultaneously enhanced photothermal performance and stability. Mater. Lett. **188**, 111–114 (2017)
51. Z. Zhang, L. Wang, J. Wang, X. Jiang, X. Li, Z. Hu, Y. Ji, X. Wu, C. Chen, Mesoporous silica-coated gold nanorods as a light-mediated multifunctional theranostic platform for cancer treatment. Adv. Mater. **24**, 1418–1423 (2012)
52. L. Feng, Y. Chen, J. Ren, X. Qu, A graphene functionalized electrochemical aptasensor for selective label-free detection of cancer cells. Biomaterials **32**, 2930–2937 (2011)
53. X. Yang, X. Liu, Z. Liu, F. Pu, J. Ren, X. Qu, Near-infrared light-triggered, targeted drug delivery to cancer cells by aptamer gated nanovehicles. Adv. Mater. **24**, 2890–2895 (2012)
54. S. Shen, H. Tang, X. Zhang, J. Ren, Z. Pang, D. Wang, H. Gao, Y. Qian, X. Jiang, W. Yang, Targeting mesoporous silica-encapsulated gold nanorods for chemo-photothermal therapy with near-infrared radiation. Biomaterials **34**, 3150–3158 (2013)
55. L. Au, D. Zheng, F. Zhou, Z.-Y. Li, X. Li, Y. Xia, A quantitative study on the photothermal effect of immuno gold nanocages targeted to breast cancer cells. ACS Nano **2**, 1645–1652 (2008)
56. M.S. Yavuz, Y. Cheng, J. Chen, C.M. Cobley, Q. Zhang, M. Rycenga, J. Xie, C. Kim, K.H. Song, A.G. Schwartz, L.V. Wang, Y. Xia, Gold nanocages covered by smart polymers for controlled release with near-infrared light. Nat. Mater. **8**, 935–939 (2009)
57. P. Shi, K. Qu, J. Wang, M. Li, J. Ren, X. Qu, pH-responsive NIR enhanced drug release from gold nanocages possesses high potency against cancer cells. Chem. Commun. **48**, 7640–7642 (2012)
58. S.E. Skrabalak, J. Chen, L. Au, X. Lu, X. Li, Y. Xia, Gold nanocages for biomedical applications. Adv. Mater. **19**, 3177–3184 (2007)
59. W.J. Cui, J.Z. Bei, S.G. Wang, G. Zhi, Y.Y. Zhao, X.S. Zhou, H.W. Zhang, Y. Xu, Preparation and evaluation of poly(L-lactide-co-glycolide) (PLGA) microbubbles as a contrast agent for myocardial contrast echocardiography. J. Biomed. Mater. Res. B **73**, 171–178 (2005)
60. H. Ke, J. Wang, Z. Dai, Y. Jin, E. Qu, Z. Xing, C. Guo, X. Yue, J. Liu, Gold-nanoshelled microcapsules: A theranostic agent for ultrasound contrast imaging and photothermal therapy. Angew. Chem. Int. Ed. **50**, 3017–3021 (2011)
61. Y.N. Qiang, L. Ling, L.J. Mei, J.T. Tong, Z.L. Xin, X.X. Liang, Preparation of gold tetrananocages and their photothermal effect. Chin. Phys. B **22**, 097502 (2013)
62. S. Huang, S. Duan, J. Wang, S. Bao, X. Qiu, C. Li, Y. Liu, L. Yan, Z. Zhang, Y. Hu, Folic-acid-mediated functionalized gold nanocages for targeted delivery of anti-miR-181b in combination of gene therapy and photothermal therapy against hepatocellular carcinoma. Adv. Funct. Mater. **26**, 2532–2544 (2016)
63. J. Chen, D. Wang, J. Xi, L. Au, A. Siekkinen, A. Warsen, Z.-Y. Li, H. Zhang, Y. Xia, X. Li, Immuno gold nanocages with tailored optical properties for targeted photothermal destruction of cancer cells. Nano Lett. **7**, 1318–1322 (2007)
64. J. Chen, C. Glaus, R. Laforest, Q. Zhang, M. Yang, M. Gidding, M.J. Welch, Y. Xia, Gold nanocages as photothermal transducers for cancer treatment. Small **6**, 811–817 (2010)
65. M.P. Melancon, M. Zhou, C. Li, Cancer theranostics with near-infrared light-activatable multimodal nanoparticles. Acc. Chem. Res. **44**(10), 947–956 (2011)
66. J. You, R. Shao, X. Wei, S. Gupta, C. Li, Near-infrared light triggers release of paclitaxel from biodegradable microspheres: Photothermal effect and enhanced antitumor activity. Small **6**, 1022–1031 (2010)
67. G. Wu, A. Mikhailovsky, H.A. Khant, C. Fu, W. Chiu, J.A. Zasadzinski, Remotely triggered liposome release by near-infrared light absorption via hollow gold nanoshells. J. Am. Chem. Soc. **130**, 8175–8177 (2008)
68. Y. Liang, J. Liu, T. Liu, Z. Chen, X. Yang, Anti-cMet antibody conjugated hollow gold nanospheres as a new nano-material for enhancing the effect of photothermal therapy. Mater. Lett. **143**, 226–229 (2015)
69. J. You, G. Zhang, C. Li, Exceptionally high payload of doxorubicin in hollow gold nanospheres for near-infrared light-triggered drug release. ACS Nano **4**, 1033–1041 (2010)

70. J. You, R. Zhang, G. Zhang, M. Zhong, Y. Liu, C.S. Van Pelt, D. Liang, W. Wei, A.K. Sood, C. Li, Photothermal-chemotherapy with doxorubicin-loaded hollow gold nanospheres: A platform for near-infrared light-trigged drug release. J. Control. Release **158**, 319–328 (2012)
71. M.P. Melancon, A.M. Elliott, A. Shetty, Q. Huang, R.J. Stafford, C. Li, Near-infrared light modulated photothermal effect increases vascular perfusion and enhances polymeric drug delivery. J. Control. Release **156**, 265–272 (2011)
72. H. Yuan, A.M. Fales, T. Vo-Dinh, TAT peptide-functionalized gold nanostars: Enhanced intracellular delivery and efficient NIR photothermal therapy using ultralow irradiance. J. Am. Chem. Soc. **134**, 11358–11361 (2012)
73. S. Wang, P. Huang, L. Nie, R. Xing, D. Liu, Z. Wang, J. Lin, S. Chen, G. Niu, G. Lu, X. Chen, Single continuous wave laser induced photodynamic/plasmonic photothermal therapy using photosensitizer-functionalized gold nanostars. Adv. Mater. **25**, 3055–3061 (2013)
74. J. Li, Y. Hu, J. Yang, P. Wei, W. Sun, M. Shen, G. Zhang, X. Shi, Hyaluronic acid-modified Fe_3O_4@au core/shell nanostars for multimodal imaging and photothermal therapy of tumors. Biomaterials **38**, 10–21 (2015)
75. L. Wang, D. Meng, Y. Hao, Y. Hu, M. Niu, C. Zheng, Y. Yanyan, D. Li, P. Zhang, J. Chang, Z. Zhang, Y. Zhang, A gold nanostar based multi-functional tumor-targeting nanoplatform for tumor theranostic applications. J. Mater. Chem. B **4**, 5895–5906 (2016)
76. X. Wang, H. He, Y. Wang, J. Wang, X. Sun, H. Xu, Active tumor-targeting luminescent gold clusters with efficient urinary excretion. Chem. Commun. **52**, 9232–9235 (2016)
77. L.V. Nair, R.V. Nair, R.S. Jayasree, An insight into the optical properties of a sub nanosize glutathione stabilized gold cluster. Dalton Trans. **45**, 11286–11291 (2016)
78. F. Zhou, B.H.Y. Feng, D. Wang, T. Wang, J. Liu, Q. Meng, S. Wang, P. Zhang, Z. Zhang, Y. Li, Cisplatin prodrug-conjugated gold nanocluster for fluorescence imaging and targeted therapy of the breast cancer. Theranostics **6**(5), 679–687 (2016)
79. J.G. Croissant, D. Zhang, S. Alsaiari, J. Lu, L. Deng, F. Tamanoi, Protein-gold clusters-capped mesoporous silica nanoparticles for high drug loading, autonomous gemcitabine/doxorubicin co-delivery, and in-vivo tumor imaging. J. Control. Release **229**, 183–191 (2016)
80. L. Li, X. Liu, C. Fu, L. Tan, H. Liu, Biosynthesis of fluorescent gold nanoclusters for in vitro and in vivo tumor imaging. Opt. Commun. **355**, 567–574 (2015)
81. X. Zhang, W. F-G, P. Liu, H.-Y. Wang, N. Gu, Z. Chen, Synthesis of ultrastable and multifunctional gold nanoclusters with enhanced fluorescence and potential anticancer drug delivery application. J. Colloid Interface Sci. **455**, 6–15 (2015)
82. W. Ge, Y. Zhang, J. Ye, D. Chen, F.U. Rehman, Q. Li, Y. Chen, H. Jiang, Facile synthesis of fluorescent au/Ce nanoclusters for high-sensitive bioimaging. J. Nanobiotechnol. **13**, 8 (2015)
83. S. Chattoraj, M.A. Amin, S. Mohapatra, S. Ghosh, K. Bhattacharyya, Cancer cell imaging using in situ generated gold nanoclusters. Chem. Phys. Chem. **17**, 61–68 (2016)
84. L. Dykman, N. Khlebtsov, Gold nanoparticles in biomedical applications: Recent advances and perspectives. Chem. Soc. Rev. **41**, 2256–2282 (2012)
85. H. Hleb, Y. Hu, R. Drezek, J. Hafner, D. Lapotko, Photothermal bubbles as optical scattering probes for imaging living cells. Nanomedicine **3**, 797–812 (2008)
86. G. Akchurin, B. Khlebtsov, G. Akchurin, V. Tuchin, V. Zharov, N. Khlebtsov, Gold nanoshell photomodification under a single-nanosecond laser pulse accompanied by color-shifting and bubble formation phenomena. Nanotechnology **19**, 015701 (2008)
87. E.Y. Hleb, D.O. Lapotko, Photothermal properties of gold nanoparticles under exposure to high optical energies. Nanotechnology **19**, 355702 (2008)